# Implementation and Evaluation of a Three-Dimensional Photometric Sampler

**Hideichi Sato, Shree K. Nayar, and Katsushi Ikeuchi**

**CMU-CS-92-148**

July, 1992

School of Computer Science
Carnegie Mellon University
Pittsburgh, PA 15213 USA





This research was conducted in the Task-oriented Vision Laboratory, Vision and Autonomous Center, School of Computer Science, Carnegie Mellon University. Image Understanding Research in the TVL is supported in part by the Westinghouse Electric Corporation and in part by the Defense Advanced Research Project Agency, DOD, through ARPA order No. 7597, and monitored by the Air Force Avionics Laboratory under contract F33615-90-C-1465.

**Keywords:** Computer vision, shape from shading, photometric stereo, roughness measurement, surface inspection

# Contents

## Abstract

The photometric sampling method extracts shape and reflectance properties of surfaces (Lambertian, specular, and hybrid) by using multiple illumination directions and a single viewing direction. In this paper, we describe a complete implementation and a performance evaluation of a three-dimensional version of the photometric sampler.

All existing shape extraction techniques that are based on photometric measurements rely on assumed surface reflection properties. We proposed a method for determining the shape of surfaces whose reflectance properties may vary from Lambertian to specular without prior knowledge of the relative strengths of the Lambertian and specular components of reflection.

The object surface is illuminated using extended light sources and is viewed from a single direction. Extended light sources make it possible to ensure the detection of both Lambertian and specular reflections. Extended sources are generated by illuminating a diffuser with a point source of light. In the 3D implementation of the photosampler, multiple extended sources are generated by distributing 36 point sources around a spherical diffuser, each light source is located at the vertex of a one-frequency icosahedron.

An extraction algorithm uses the set of image brightness values measured at each surface point in order to compute orientation as well as the strengths of the Lambertian and specular reflection components. In order to increase the accuracy in measured orientations and reflectance parameters, we have developed a calibration method to overcome the the difference between the theoretical and the actual distributions of extended source brightness.

The experimental conducted on Lambertian surfaces, specular surfaces, and hybrid surfaces show high accuracy in both estimated orientations as well as reflectance parameters. We have demonstrated the ability of our system to detect cracks, and reflectance parameter variances in several industrial objects.

# 1 Introduction

Shape from shading [4, 6, 11], photometric stereo [16, 5, 2], and local shape from specularity [3] are examples of techniques that extract three-dimensional shape information from photometric measurements. All of these techniques rely on prior knowledge of surface reflectance properties. The reflectance properties are either assumed, or measured using a calibration object of known shape. In many real-world applications, such as those involving surfaces of different reflectance characteristics, the calibration approach is not a practical one. Therefore, the existing shape extraction methods are often used by assuming surface reflectance to be either Lambertian or specular. Many surfaces encountered in practice are hybrid in reflectance; their reflectance models are linear combinations of Lambertian and specular models. Therefore, Lambertian and specular models are only limiting instances of the hybrid model. It is desirable to have a method that is capable of extracting the shape of hybrid surfaces as well as Lambertian and specular ones.

In many industrial applications, surface polish and roughness are found to be important inspection criteria. In such cases, surface reflectance properties may be interpreted as measures of surface polish and roughness. Furthermore, reflectance properties may be used to segment an image into different regions; each region may be regarded as a different surface to aid the process of inspection. For these reasons, it would be of great value to have a technique that could, in addition to determining shape, also estimate the reflectance properties of each surface point [8, 15, 7].

We have presented the photometric sampling [9] for determining the shape of objects whose surfaces may be Lambertian, specular, or hybrid. The method used extended light sources to illuminate an object surface. A sequence of images of the object are generated by actively controlling an array of extended sources, which are located on a plane passing through the object. Surface orientation was extracted without prior knowledge of the relative strengths of the Lambertian and specular reflection components. However, we had only implemented and demonstrated 2D version of the photometric sampling method: all of the light sources were located in the same plane and only objects with translated symmetry could be handled.

This paper describes the extension of our previous work, a 3D version of the photometric sampling which can handle surfaces of arbitray shape. Surface orientation is extracted without prior knowledge of the relative strengths of the Lambertian and specular reflection components. The method also determines the parameters of the reflectance model at each surface point. The experimental

results have shown high accuracy in extracted object shape and surface reflectance properties.

# 2 Photometric Sampling

## 2.1 Basic Photometric Function

The brightness distribution in the image of an object is closely related to the reflectance properties and shape of the object surface, and the characteristics of the light source used to illuminate the object. The basic photometric function is defined as one that relates image brightness to the surface reflectance and the imaging geometry: surface orientation, viewer and source direction [1].

Consider the illumination of an object by a point source of light. The point source emits light in all directions. Light energy reflected by the surface in the direction of the camera causes an image of the surface to be formed in the camera. For a given orientation of the surface and direction of the point source, the amount of light energy reflected by the surface in a particular direction is determined by its reflectance properties. The photometric function of a large number of surfaces comprises three components, namely, the Lambertian (diffuse), the lobe (rough) component, and the specular (gloss) component [10]. Figure 1 shows the relationship between these three components and the imaging geometry.

Our photometric sampling method handles smooth surfaces [2]. Then, we can neglect the specular lobe component and express the brightness at an image point as:

$$I = IL + IS. \tag{1}$$

where $IL$ and $IS$ denotes the image brightness due to the Lambertian component and the specular spike component, respectively.

The Lambertian brightness $IL$ results from the non-homogeneous nature of the layers that constitute the object surface. Light rays penetrating the surface undergo multiple refractions and reflections at the boundaries between surface layers and reemerge near the point of entry with a variety of directions. These surfaces appear equally bright from all directions; the brightness $IL$ is independent of the viewing direction.

[1] The photometric function is similar to the image irradiance equation [4]; both represent the relationship between the image brightness and the imaging geometry. The reader may, therefore, regard the photometric function as an unnormalized image irradiance equation.

[2] More precisely, we assume that the surface roughness measure $g$ is much smaller than 1. See [10].

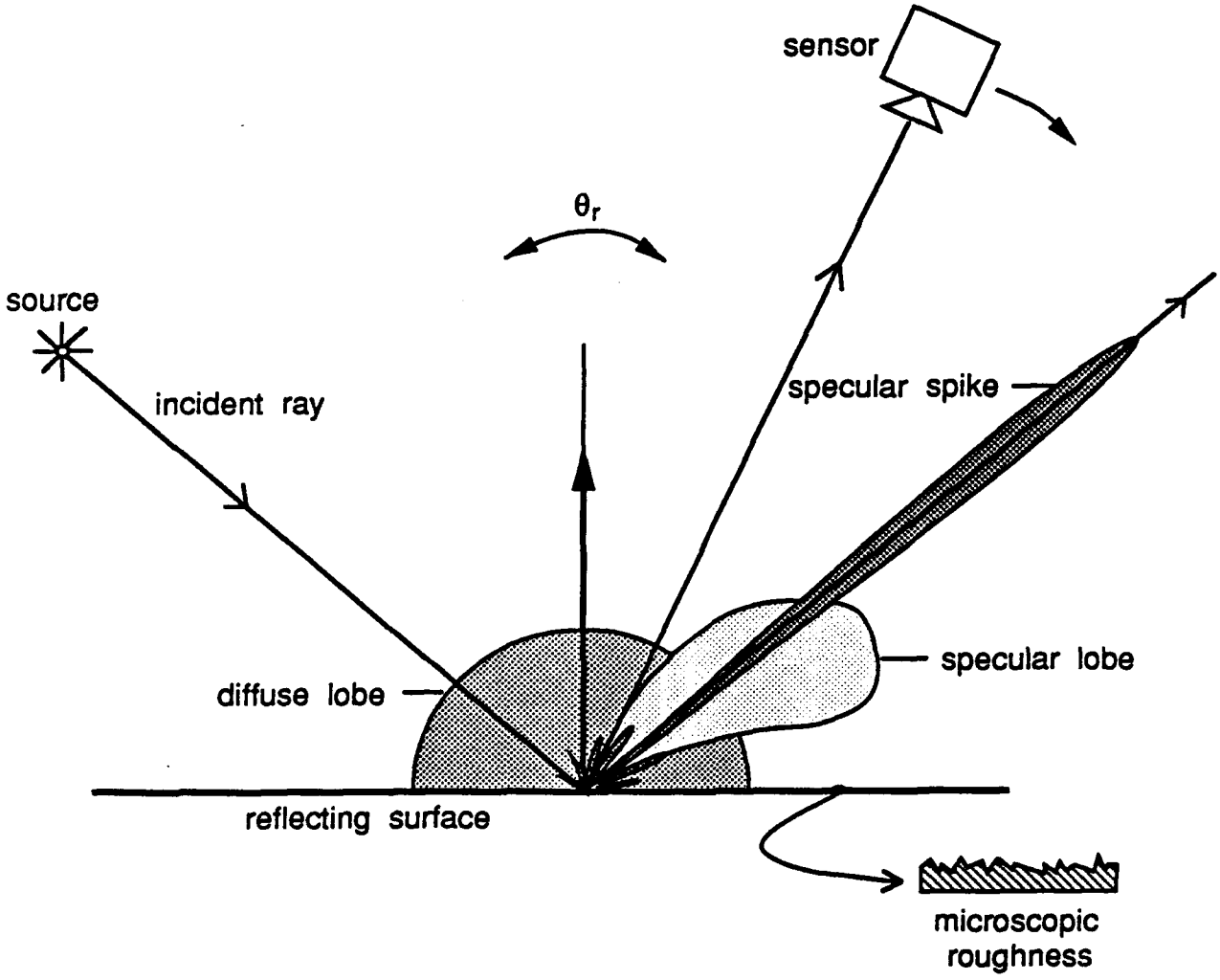


Figure 1: Polar plots of the three reflection components as the function of the viewing angle for a fixed source direction

The brightness of a Lambertian surface point is proportional to the energy of received incident light. The amount of light energy falling on the surface element is proportional to the area of the surface element as seen from the point source position, often referred to as the foreshortened area. The foreshortened area is a cosine function of the angle $\beta$ between the surface orientation direction $\vec{N}$ and the source direction $\vec{S}$ from the surface point, where $\vec{N}$ and $\vec{S}$ are unit vectors. Thus, the Lambertian brightness component $IL$ may be written using these vectors as:

$$\begin{aligned} IL &= A\cos\beta \\ &= A\,\vec{S}\cdot\vec{N} \end{aligned} \tag{2}$$

where $A$ is a constant representing ratio of absorption between the incoming energy and emitting energy, the Lambertian albedo.

The specular spike brightness $IS$ results from the light rays that are unable to penetrate the surface layer and reflected back to the air. It is represented by a very sharp function of the source direction $\vec{S}$ with respect to the viewer and the surface orientation. We can approximate it by a unit impulse function:

$$IS = B\,U(\vec{N},\vec{S}) \tag{3}$$

where:

$$U(\vec{N},\vec{S}) = \begin{cases} 1 & \text{if } \vec{N} = \frac{\vec{S}+\vec{V}}{|\vec{S}+\vec{V}|} \\ 0 & \text{otherwise} \end{cases}$$

and $B$ is the specular spike and $\vec{V}$ is a unit normal representing the viewer direction.

The photometric sampling method determines orientation and reflectance under a fixed viewer direction. We can set up the viewer center coordinate system so that this viewer direction coincides to the $Z$ axis; $\vec{V}$ is denoted as $(0, 0, 1)^t$. We can represent source and surface orientation directions with respect to this coordinate system.

By moving the source directions around the object, we can vary the source direction without changing the surface orientation and reflectance parameters.

It is important to note that varying the source direction does not change the orientation and reflectance parameters. Therefore, even though the orientation and reflectance parameters are unknown, we can treat them as constants in equation 1. For this reason, we will often refer to the basic photometric function as $I(\vec{S})$, a relation between image brightness and source direction.

We will denote the surface orientation direction which satisfies $\vec{N} = \frac{\vec{S}+\vec{V}}{|\vec{S}+\vec{V}|}$ for a given source direction as the *specular surface direction* of the source direction, $\vec{N}_s(\vec{S})$. The source direction which satisfies this equation for a given surface direction as the *specular source direction* of the surface, $\vec{S}_s(\vec{N})$.

Figure 2 shows plots of the basic photometric function as the function of the moving light source in the viewer centered coordinate system.

## 2.2 Extended Light Source

Numerous point source illumination methods [2, 12, 16, 14], have been proposed that extract the shape of either Lambertian or specular surfaces. A problem associated with the use of point sources is that the specular component of reflection is not detected unless the $\vec{N} = \vec{N}_s(\vec{S})$. To detect specular reflections from surface points of all orientations, an infinite number of point sources need to be positioned around the surface. Such an approach is not practical.

We will use extended light sources to illuminate the object surface [5]. Unlike a point source, an extended source emits light from an area of points rather than a single point. This characteristic of an extended source reduces the number of necessary sources to detect specular components of reflection.

In order to determine shape and reflectance parameters of hybrid surfaces, both specular and Lambertian reflections must be captured in the measured brightness. However, experiments have shown that for point source illumination, it is difficult to measure both Lambertian and specular reflections without changing the sensitivity of the measuring device. Image brightness due to specular reflections have been observed to be much higher than the brightness resulting from Lambertian reflections.

For extended source illumination, a specular surface element of a given orientation will reflect light from a small area of the extended source into the camera. On the other hand, a Lambertian surface element of the same orientation reflects light from all points of the extended source. Due to this integration effect, under an extended source, the the relative brightness of a Lambertian component to those specular component under an extended source is much greater than under a point source due to the integration effect. Therefore, an extended light source makes it possible to detect both Lambertian and specular reflections without changing the sensitivity of the sensor.

We generate an extended source by illuminating a sphere made of light-

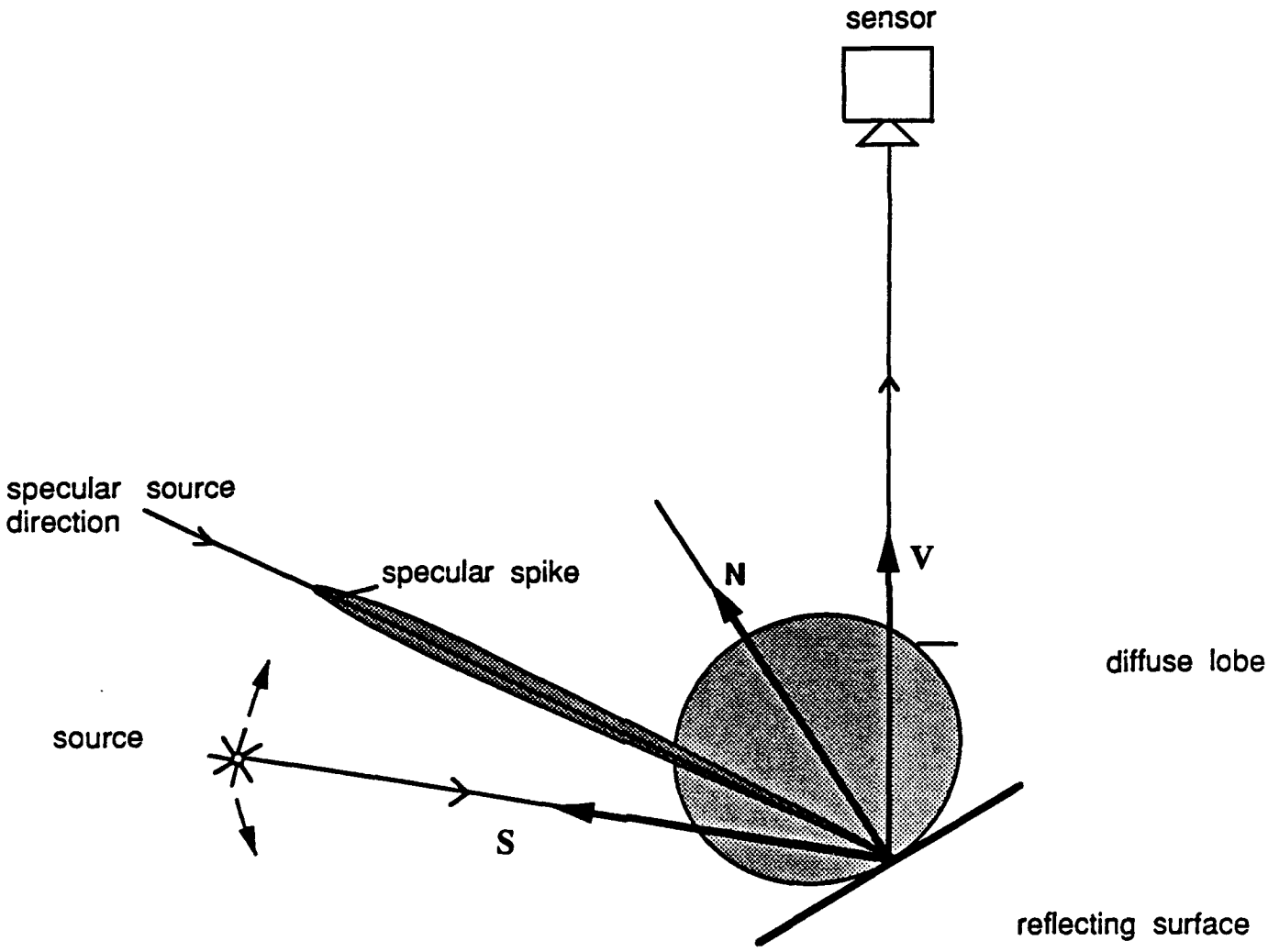


Figure 2: Polor plots of the Lambertian and specular spike components of the moving light source.

diffusing material with a point source of light. The object is placed at the center of the spherical diffuser and is viewed by the camera through a hole in the diffuser. In the following discussion, the origin of the viewer center coordinate system is defined as the sphere center, and the Z axis corresponds to the optical axis of the TV camera. All vectors, such as $\vec{S}$ and $\vec{N}$, are defined in this viewer centered coordinate system.

Each point source illuminates the spherical diffuser, and the illuminated area on the spherical diffuser acts as an extended light source. Brightness at any point on the sphere, $\vec{P}$, is described by the brightness distribution function of the extended light source, $L(\vec{P}, \vec{S})$, given by the illumination geometry. The brightness distribution function has the following characteristics:

- the position of an extended source is defined as the direction, $\vec{S}$, of the point source which generates the extended source,
- the brightness distribution function has a non zero area. It is bounded by a circle whose radius is $\alpha$ and whose center is the position of the extended source. In other words, $L = 0$ for $\beta > \alpha$, where $\beta = cos^{-1}(\vec{S} \cdot \vec{P})$. We will refer to $\alpha$ as the *termination angle* of the extended light source,
- the brightness distribution function is rotational symmetric with respect to the source position $\vec{S}$,
- its magnitude decreases as $\vec{P}$ deviates from $\vec{S}$.

## 2.3 Photometric Function for Extended Sources

We will modify the point source illumination photometric function (Eq. 1) into an extended source illumination photometric function. An extended source may be thought of as a collection of point sources. Each point source has a brightness that is dependent on its position in the extended source. The brightness of light reflected by an object surface that is illuminated by an extended source may be determined by computing the integral of the light energy reflected from all points on the extended source. Therefore, the modified photometric function $I'(\vec{S})$ is determined by convolving the basic photometric function $I(\vec{S})$ with the brightness distribution function $L(\vec{P}, \vec{S})$.

For a surface point of orientation $\vec{N}$ the Lambertian component $IL'$ of the modified photometric function is determined as:

$$\begin{aligned} IL' &= \int\int IL(\vec{P})L(\vec{P},\vec{S})d\vec{P} \\ &= \int\int A\,(\vec{N}\cdot\vec{P})\,L(\vec{P},\vec{S})\,d\vec{P} \\ &= A'\vec{N}\cdot\vec{S} \end{aligned} \tag{4}$$

The specular component of the modified photometric function is proportional to the brightness of the extended source at the specular source direction, $\vec{S}_n(\vec{N})$. Therefore, the photometric function for surface illumination by the extended source is:

$$I' = A'\vec{N}\cdot\vec{S} + B'\,L(\vec{S}_n(\vec{N}),\vec{S}) \tag{5}$$

Eq. 5 is the modified photometric function that relates image brightness to surface orientation, surface reflectance, and source position for extended source illumination. In the equation, surface orientation and reflectance parameters are unknown, but constant, for a given surface point. For this reason, we will frequently refer to the modified photometric function as a relation between image brightness and extended source direction, $I'(\vec{S})$.

## 2.4 Sampling

The process of measuring image brightness for different source directions is equivalent to sampling the modified photometric function, $I'(\vec{S})$, at various $\vec{S}_i$. Samples of the photometric function may be obtained by moving an extended source around the object and taking images of the object for different source positions. An alternative approach would be to distribute an array of extended sources around the object such that each source illuminates the object from a different direction. The entire array of extended sources may be scanned by sequentially activating each source one at a time and taking an image. Therefore, the scanning process results in a set of brightness, $I_i : i = 1,\ldots,M$, measured at each point on the object surface. $M$ equals the number of extended sources.

The number of samples measured at each surface point is determined by the termination angle $\alpha$. As stated earlier, in order to extract the shape and reflectance parameters of hybrid surfaces, both Lambertian and specular components of image brightness must be detected. Since we have used a unit impulse specular reflection

model, the area of the photometric function that contains specular brightness is bounded by an $\alpha$ radius circle.

Uniform sampling of the photometric function may be obtained by distributing extended sources in a tessellation that results from projecting onto the unit sphere a regular polyhedron whose center coincides with that of the sphere[1]. A higher frequency polyhedron which consists of triangular faces can be used [13] for a smaller meshed tessellation.

We will use a polyhedron whose edge length projects to an arc length equivalent to $\alpha$. This spacing allows the photometric function to be uniformaly sampled at an interval equal to $\alpha$. Under this sampling interval, one and only one spherical triangle gives three non-zero specular brightnesses. (See Figure 3.) We will use this constraint for designing a recovery algorithm. We will refer to this triangle and the constrain as the *specular triangle* and the *sampling constraint*, respectively.

## 2.5 Extracting Shape and Reflectance of Surfaces

Given the set of image brightness values, $I_i : i = 1, \ldots, M$ we want to determine the surface orientation, $\vec{N}$, and the strengths, $A'$ and $B'$, of the Lambertian and specular components of reflection. The shape and reflectance properties extracted at each surface point are solely based on the image brightness recorded at that point. The surface property values assigned to a surface point are not influenced by the image brightness measured at neighboring points. We will first develop techniques to extract surface orientations of purely Lambertian and purely specular surfaces. Later, these techniques will be used as tools to extract surface orientations and reflectance properties of hybrid surfaces.

**Lambertian Surfaces** Consider the case where the surface of an object is known to be purely Lambertian, and the shape of the object is to be determined. The photometric samples for a Lambertian surface may be written as:

$$I_i = A' \vec{N} \cdot \vec{S}_i \tag{6}$$

We would like to compute the surface orientation, $\vec{N}$, and and the strength, $A'$, of the Lambertian reflection component. These variables may be estimated by fitting the equation to the set of image brightness, $I_i : i = 1, \ldots, M$ and extended source directions, $\vec{S}_i : i = 1, \ldots, M$, using the least square fitting method.

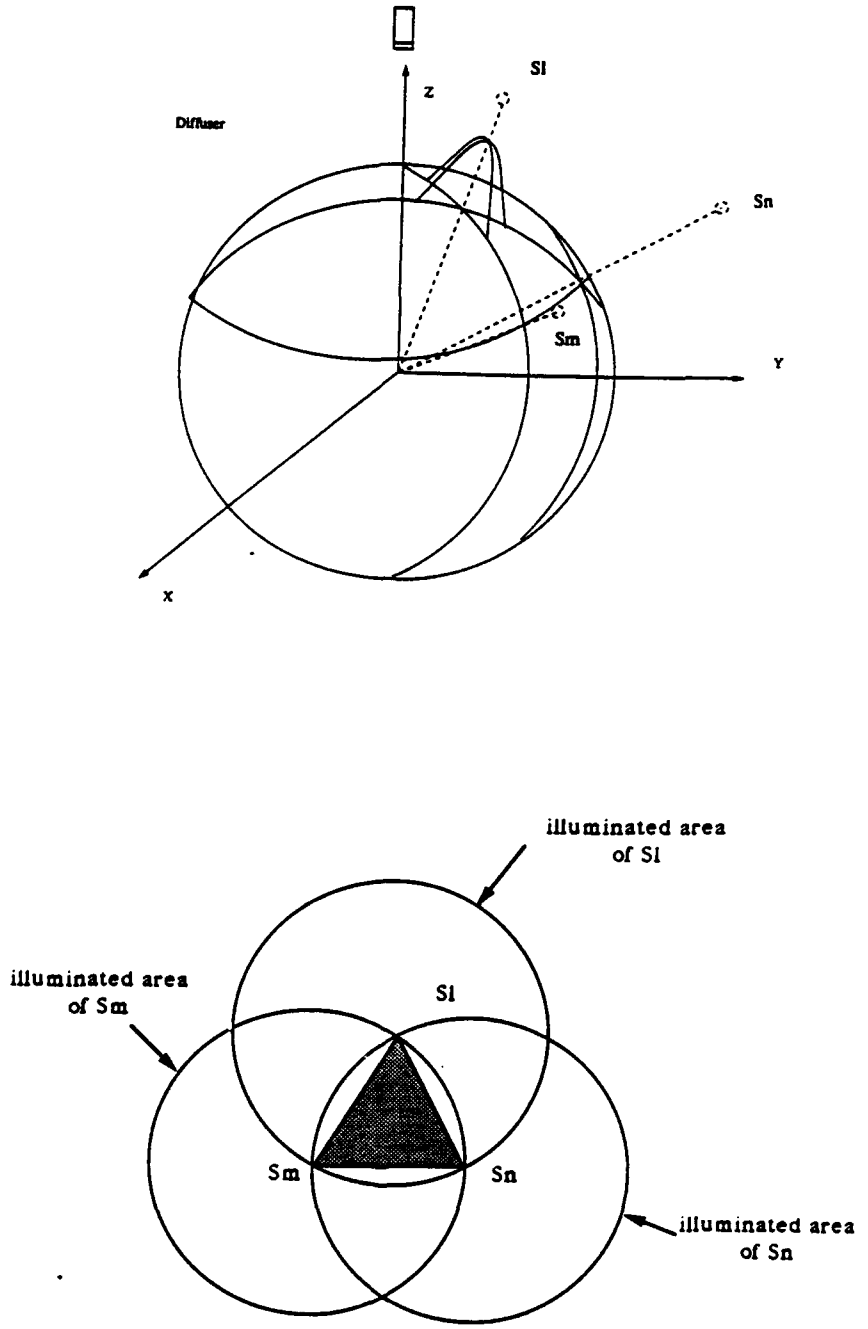


Figure 3: Sampling constraint: one and only one spherical triangle produces all three non-zero specular brightness values.

**Specular Surfaces** Now consider the case where the object surface is known to be purely specular, and the shape of the object is to be determined. From the sampling constraint, we can assume that only three brightness values are non-zero, and the corresponding three directions form a specular triangle.

Given the image brightness set, $I_i : i = 1, \ldots, M$, at a surface point, the three non-zero image brightness values in the set are first determined. These three values, $I_l, I_m, I_n$, and their corresponding source directions, $\vec{S}_l, \vec{S}_m, \vec{S}_n$ must satisfy the following four equations:

$$\begin{aligned} I_l &= B'L(\vec{S}_n(\vec{N}), \vec{S}_l) \\ I_m &= B'L(\vec{S}_n(\vec{N}), \vec{S}_m) \\ I_n &= B'L(\vec{S}_n(\vec{N}), \vec{S}_n) \\ |\vec{N}| &= 1 \end{aligned} \tag{7}$$

By solving these four equations, we can determine the surface orientation, $\vec{N}$, and specular strength, $B'$ at each point. In the actual implementation, however, we use a lookup table to convert a triple of brightness values into a unique surface orientation [5].

**Hybrid Surfaces** A large number of surfaces may be classified as hybrid surfaces whose photometric functions are linear combinations of Lambertian and specular components. The hybrid surface class includes plastic surfaces and painted smooth surfaces. We will develop an algorithm to recover the Lambertian strength and specular strength, and surface orientation of a hybrid surface. The extraction algorithm is developed based on the sampling constraint.

This method assumes that all the image brightness does not contain any specular component. We will determine the surface orientation, $\vec{N}_{lamb}$, and the Lambertian strength, $A'$, using the least square fitting method as mentioned above.

Then, we will calculate the theoretical brightness, $I'_i : i = 1, \ldots, M$, for all source directions using $A'$, $\vec{N}_{lamb}$, and $S_i : i = 1, \ldots, M$. By subtracting theoretical brightness values from the observed ones, we obtain residual brightness values $\Delta I_i = I'_i - I_i$. The residual brightness represents specular brightness. The sampling constraint guarantees that only three residual values contain non-zero values. By finding these residual brightness, we can identify the specular triangle. Using the three brightness residual brightness and the specular triangle, we can determine the surface orientation, $\vec{N}_{spec}$, and the specular strength, $B'$, by using the same procedure as was used for specular surfaces.

Third, we will use the least square fitting method on the remaining brightness values and redetermine the surface orientation, $\vec{N}_{lamb}$, and the Lambertian strength, $A'$. Using these values, we will recalculate the brightness residues. We find the three largest residues and redetermine the specular triangle. Then, we again estimate the specular strength, $B'$, and surface orientation, $\vec{N}_{spec}$, from these residues.

We have two surface orientations given by two different methods (Lambertian and specular). We compute a weighted average of both surface orientations into a single value based on the ratio of Lambertian and specular strength:

$$\vec{N} = \frac{A'\vec{N}_{lamb} + B'\vec{N}_{spec}}{A' + B'}.$$

# 3 Three-Dimensional Photo-sampler Apparatus

## 3.1 Designing the Apparatus

We produce an extended source by illuminating a spherical diffuser with a point source. The object is placed at the center of the spherical diffuser. Point light sources are distributed uniformly over the diffuse sphere. Each point source illuminates a part of the diffuser, and that part acts as an extended source. This illuminated area on the diffuse sphere is referred to as the *effective area* of the extended source. The effective area is bounded by a spherical circle whose radius is the termination angle $\alpha$ and whose center is the light source direction.

The termination angle determines the number of point sources necessary to cover the entire surface of spherical diffuser. In terms of efficiency, we prefer a larger $\alpha$ value. A large $\alpha$ needs fewer sources to cover the spherical surface. But, a large $\alpha$ degrades the resolution of the surface orientation measurements, because the gradient of extended sources become flat. A smaller $\alpha$ gives a better surface orientation resolution because of the steep gradient of extented sources. On the other hand, the area of the extended source becomes smaller. We would require more sources. A smaller $\alpha$ also makes the Lambertian surfaces relatively darker than the specular surfaces. This makes it difficult to extract the Lambertian component. From several experiment, we select 40° as the optimal termination angle: $\alpha = 40°$. This configuration of point light source distribution can be realized by locating point sources at each vertex of one frequency icosahedron. This requires 42 light sources.

The distance $H$ between a point source and the surface of the diffuser is related to the termination angle $\alpha$:

$$cos\alpha = \frac{R}{R+H}, \tag{8}$$

where $R$ denotes the radius of the diffuser. See Figure 4. Therefore, once we determine the termination angle, $\alpha$, we can determine $H$ as $H = \frac{1-cos\alpha}{cos\alpha}R$

By using, $R$ and $H$ we can express the brightness distribution function of an extended light source as

$$L(\vec{P},\vec{S};R,H) = \frac{C\,[(R+H)(\vec{S}\cdot\vec{P}) - R]}{[(R+H-R\,(\vec{S}\cdot\vec{P}))^2 + (R(1-(\vec{S}\cdot\vec{P})^2)]^{\frac{1}{2}}} \tag{9}$$

where $\vec{P}$ denotes a unit vector to a point on the diffuse surface from the sphere center and $\vec{S}$ denotes the point light source direction from the sphere center.

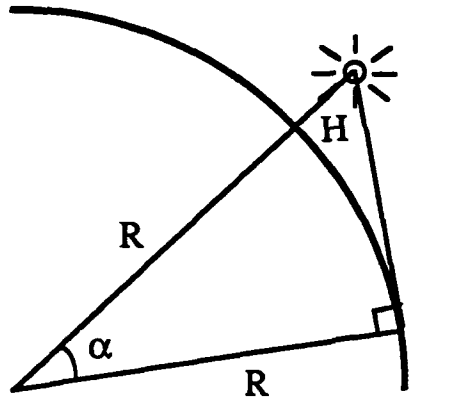


Figure 4: The relationship between $\alpha$ and $H$

Figure 5 shows a photograph of the experimental device. A 355.6mm (14-inch) diameter lamp shade is used as the spherical diffuser. Extended light sources are generated on the diffuser's surface by illuminating it with 36 60W frosty incandescent light bulbs. The bulbs are located at 36 of the 42 vertices of one-frequency icosahedron [3]. The object is placed at the center of the diffuser and is viewed by a camera through a 25.4mm (1-inch) diameter hole in the surface of the diffuser. The complete imaging system, comprise of lenses and camera, has a physical resolution of 0.5mm (0.002 inches) per pixel width.

## 3.2 System Parameters

The system parameters needed to describe the apparatus in details include: light source directions, brightness distribution parameters, and device characteristic parameters. These parameters will be used for determining shape and reflectance properties of unknown objects.

[3] A small section of the bottom hemisphere of the diffuser is not illuminated as light sources. This area is not observable from the TV camera.

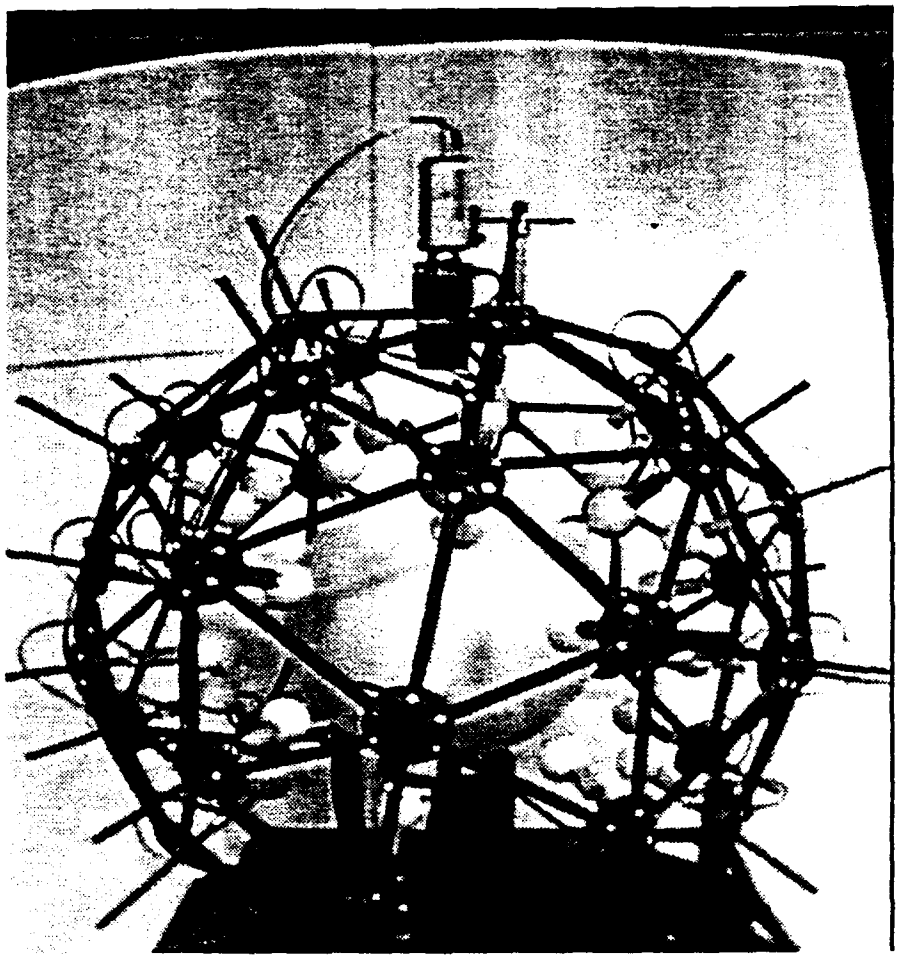

Figure 5: Photograph of the experimental apparatus.

- The *light source directions* represent directions of the center of the light sources denoted by $\vec{S}_i : i = 1, \ldots, 36$. Figure 6 shows the number of the light sources and their locations.

- The *brightness distribution parameters*, $C, H, D$, and $\sigma$, characterize the shape of the brightness distribution of a light source on the diffuser. Here the function is expressed by

$$L'(\vec{P}, \vec{S}; R, H) = \frac{C\,[(R+H)(\vec{S}\cdot\vec{P}) - R]}{[(R+H-R(\vec{S}\cdot\vec{P}))^2 + R^2(1-(\vec{S}\cdot\vec{P})^2)]^{\frac{3}{2}}} + D\exp\left(-\frac{(cos^{-1}(\vec{S}\cdot\vec{P}))^2}{2\sigma^2}\right) \quad (10)$$

For an ideal diffuser, the first term in the above the equation is accurate. However, since the sphere is not an ideal Lambertian diffuser, we add a Gaussian function to compensate this discrepancies. $C$ and $D$ represent the strength of the Lambertian and Gaussian functions, respectively. $H$ and $\sigma$ are related with the width of the Lambertian and Gaussian functions, respectively.

- Device characteristic parameters
  - The *base value for specular surfaces* ( $E_{spec}$ ) represents the increase in brightness due to interreflections inside the diffuser. We assume that this increment is independent on surface orientations.
  - The *base value for Lambertian surfaces* ($E_{lamb}$) represents the increase in brightness on Lambertian surface due to interreflections inside of the diffuser. We assume that this increment is also independent on surface orientations. This factor corresponds to the integration of the previous factor over the hemispherical directions.
  - The *light source brightness for the pure Lambertian surface* ( $A'_{max}$ ) represents the brightness that an effective point source would have, in order to produce the same brightness as an extended source. Theoretically, this value corresponds to the integration of Eq.10 over the effective illuminated area of an extended source. We determine this value by calibration for the sake of accuracy.
  - The *base value due to defocus effect* ($E_{def}$) represents the increase in brightness over the entire image because the camera observes a part of the diffuser and blurs that part over the image.

## 3.3 Calibration

We determine the system parameters and lookup tables by a calibration method. The system parameters, except for $E_{def}$, are determined for each extended light source. The lookup tables are determined for each triangle on the one-frequency icosahedron.

This calibration method takes a series of images of a specular sphere and a Lambertian sphere, and determine the parameters and tables. The light source directions, brightness distribution parameters, base value for specular surfaces,

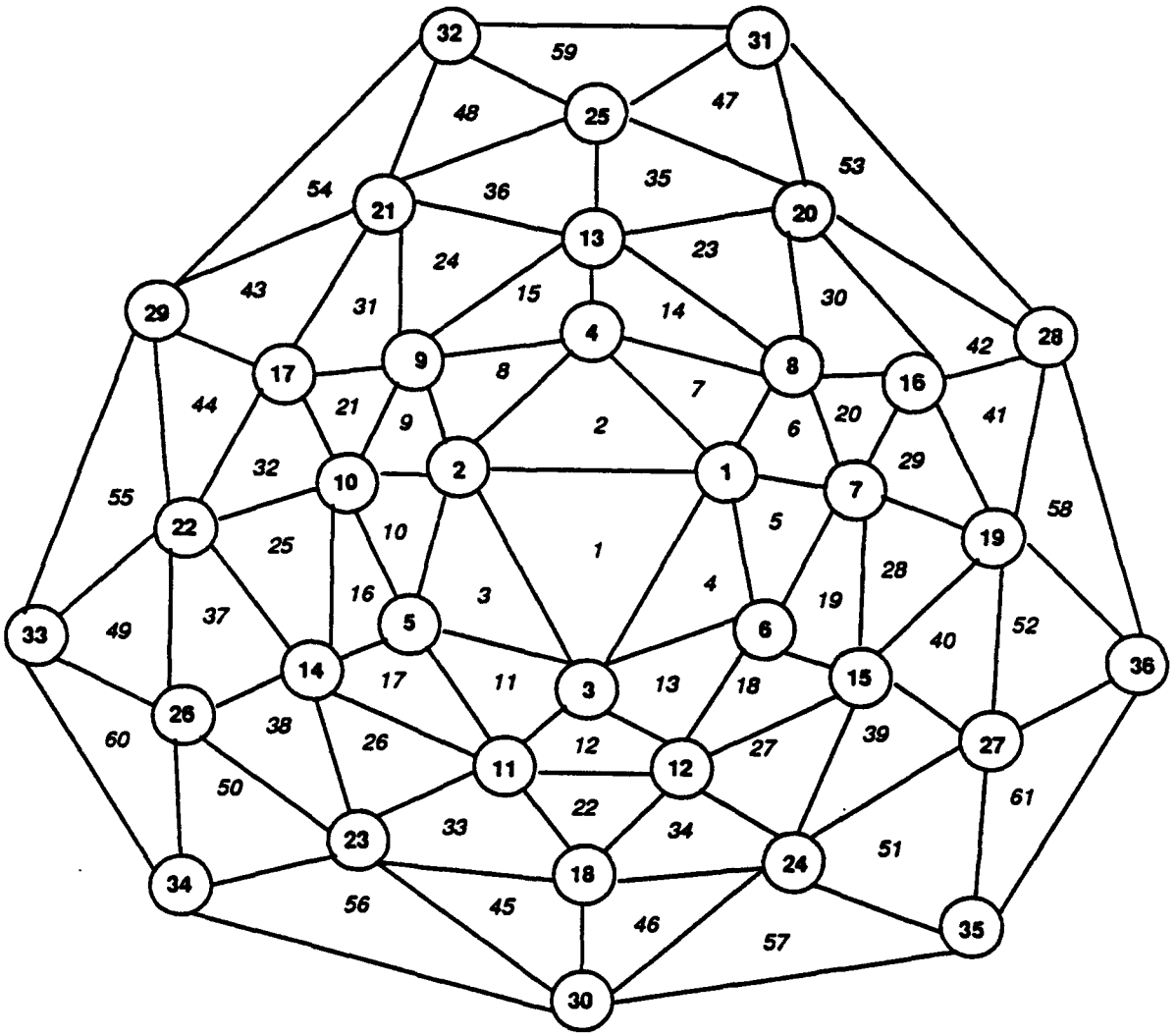


Figure 6: Map of the distribution of light sources

and the base value for the defocus effect are determined by processing 36 images of a specular sphere under the 36 extended light sources. The lookup tables are also constructed using 36 images of the specular sphere. The light source brightness for the pure Lambertian surface and base value for the Lambertian surfaces are determined by processing 36 images of a Lambertian sphere under the 36 extended light sources.

### 3.3.1 Device characteristic parameters

**Light source directions** We will repeat the following procedure for all 36 light sources. First, we turn on a light source and take an image of the specular sphere. Then, we get the maximum brightness around the image point estimated as the light source direction by the specification of the device. Third, we make a binary image using a threshold which equals 90 % of the maximum brightness, and swell the image by 3 pixels to avoid the influence of defects, stain, and dust. The direction of the light source is estimated as the center of the binary region. This estimation will be used as the initial value for the more precise calibration. Figure 7 shows the distribution of such binary areas extracted on the specular ball plotted on a plane.

**Base values for specular surfaces** Theoretically, the brightness distribution function, Eq.10, should give zero brightness outside of the effective area of an extended source. However, interreflections inside the diffuser illuminate the whole diffuser. This produces a certain brightness in areas outside of the effective area. (See Figure 8.) The interreflections depend on the shape and material of the diffuser, and the direction of the extended source. Since this brightness is about 1 % of the maximum value of the extended light sources, we neglect the differences between the light sources and assume it a constant over all the directions. In other words, we assume that we will observe a uniform increment in brightness over an image.

We obtain this base value from the difference in brightness of a point on the camera hole image and a point under the diffuser on the specular ball. Note that we should use a light source far from the camera in order to avoid the defocus effect stated later.

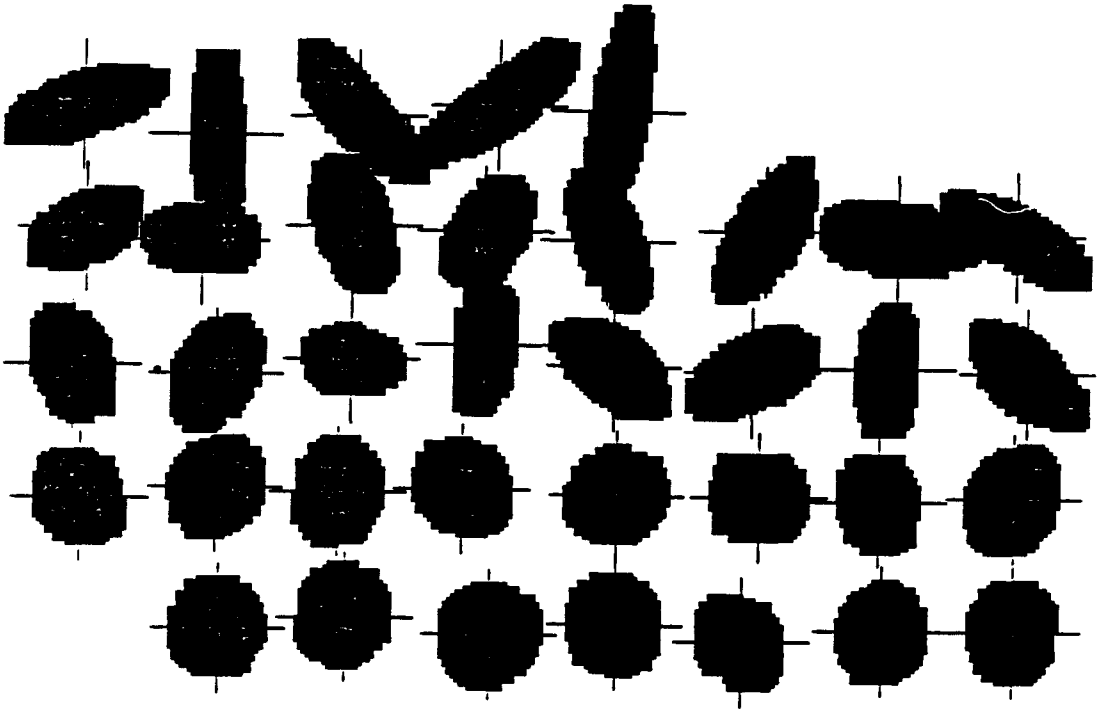

Figure 7: Binary area of light sources

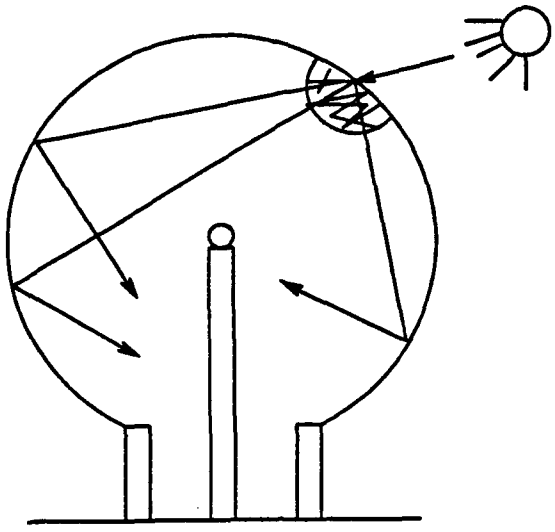

Figure 8: Interreflection in the diffuser

**Base values for the defocus effect** Because of the insufficient size of the camera hole on the diffuser, defocused parts of the diffuser get into the view of the camera [4]. This causes an increase in the brightness of the whole images.

The images under light sources near the camera have this effect much stronger than those under the far sources. Thus, we measure the defocus effect at each light source independently. We take a specular ball image under a light source. Brightness corresponding to the outside of the effective area of the light source has non-zero brightness. This brightness is caused by interreflection and defocus. In order to measure the non-zero outside brightness, we take an average of the two darkest values, among four orthogonal brightness values, along a large circle (in our case, 0.85% of the radius of the specular sphere image). We assume that the two darkest values are from outside zero-brightness. Then, we subtract the base value for specular surfaces (interreflection), determined in the previous step, from this value to get those due to the defocus effect.

[4]Reader may consider if we use a wider hole we can avoid this effect. However, a wider hole increase a hole region in specular image, and should be avoide.

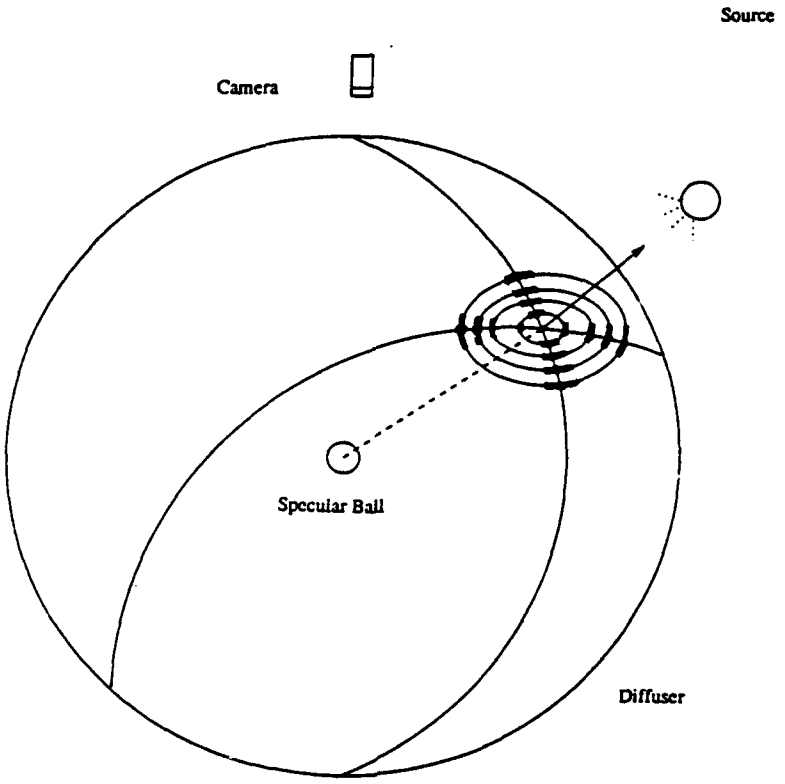


Figure 9: Sampling the intensities on the diffuser

### 3.3.2 Brightness distribution parameters

The brightness distribution parameters $C, H, D, \sigma$ characterize the shape of the brightness distribution on the diffuser. By sampling the real brightness distribution on the diffuser and fitting them to Eq. 10, we will determine these parameters. Since these parameters are unique to each light source, we will repeat the following procedure at each light source. For this calibration, we use 36 images of a specular ball under 36 light sources.

We will sample real brightness at each 3.6° interval within 36° limits along the longitudinal and the perpendicular great circle intersecting at the light source direction. At each sampling angle, we search the maximum brightness within 20° along the arc perpendicular to the sampling circle to minimize the effect of defects, stain and dust on the sampling sphere. (See Figure 9.)

By fitting the equation to the two sets, longitudinal and perpendicular, of

sampled brightness, two sets of parameters $C, H, D, \sigma$, and $\delta\theta$ are determined. Then, these two sets of parameters are averaged. Here, $C, H, D, \sigma$ are the same as those in Eq. 10 and $\delta\theta$ denotes the difference between the real and the estimated light source direction.

Each fitting process is executed in the following three steps. The first step determines the parameters for the Lambertian component, $\delta\theta, C, H$, and the second step determines those for the Gaussian component, $D$ and $\sigma$. The last step adjusts the relative strength, $C$ and $D$ so that the difference between the real one and the one described by these parameters is minimized.

The first step approximates the brightness distribution by the Lambertian components of Eq. 10 and determines the parameters, $\delta\theta$, $C$ and $H$ by using a non-linear least square fitting method. Using $H$ given by the device dimension and $D$ given by the maximum brightness value, the method obtains the $\delta\theta$ which gives the minimum error among the possible $\delta\theta$ values, $\pm 5°$ limits around the estimated light source direction and $0.1°$ intervals. Then, the method determines the height $H$ that gives the minimum error under the $C$ given by the maximum brightness. Finally, using these $H$ and $C$ as the initial values, the method determines the optimal $H$ and $C$ for the Lambertian component of Eq. 10 by the Gauss-Newton non-linear least square fitting method, iteratively.

The second step approximates the brightness distribution by the Gaussian component of Eq. 10 and determines the parameters, $D$ and $\sigma$ of Eq. 10. $D$ and $\sigma$ are determined by the Gauss-Newton non-linear least square fitting method. The initial value of $D$ is given by the maximum brightness value. The initial value of $\sigma$ is chosen so that the Gaussian component gives the same value as the one given by the Lambertian component at $9° = 0.1571$ *radian*. Namely, $\sigma = \frac{0.1571}{\sqrt{\log \frac{B}{L_0}}}$, where $L_0$ denotes the brightness at 9° from the light source direction.

The third step adjusts the ratio between the Lambertian and Gaussian components. Fixing all parameters except $C$ and $D$, we obtain these two parameters by using the least square fitting method. Figure 10 shows some of the brightness distribution function superimposed on the measured brightness.

### 3.3.3 Lookup table for surface orientations given specular component

A specular surface obeys the law of reflection and gives the brightness of an extended source at the specular source direction. From observing a triple of these brightness given by three different extended sources, we can determine the surface

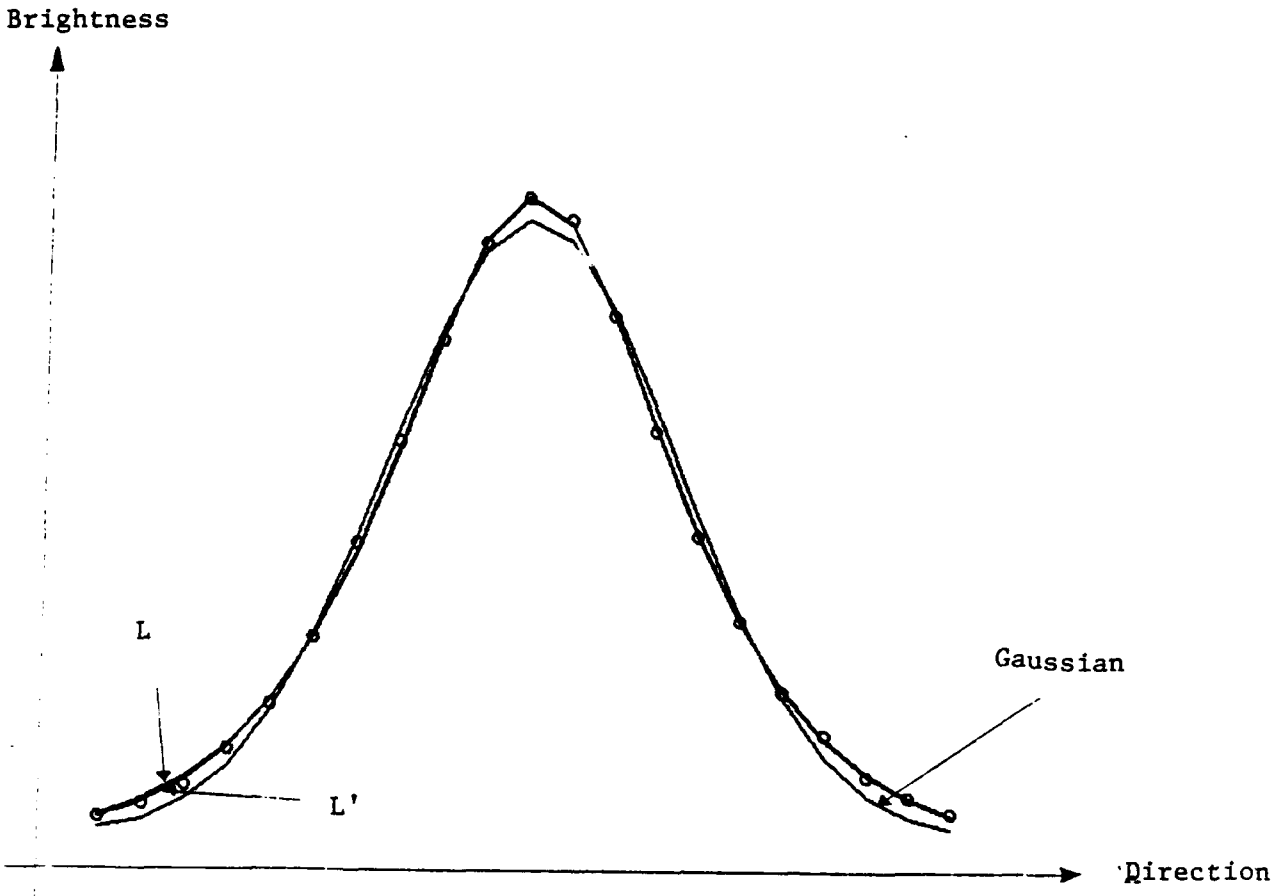


Figure 10: Brightness distribution function

orientation of the surface as described in section 2.5.

The device consists of many triangular tessellations. Within one triangular tessellation, the effective areas of three extended light sources overlap with each other. We will make the lookup table at each triangular tessellations.

We will construct a lookup table to convert a triple of brightness values to a surface orientation analytically. Here the axes of the three dimensional table correspond to three brightness values, and each cell of the table contains a surface orientation corresponding to a triple.

We sample orientation over a triangular tessellation. At each sampled orientation, we can calculate the three brightness values using Eq. 10 analytically. Here the parameters for the equation are given by the calibration method in the previous section. Then, we place the corresponding surface orientation at the cell of the table, corresponding to the calculated triple of the brightness. In order to avoid null spaces in the lookup table due to the insufficient sampling, we interpolate and extrapolate the contents of the table.

### 3.3.4 Light source brightness

The light source brightness for the pure Lambertian surface, $A'_{max}$, and the base value for the Lambertian surface. $E_{lam}$, are obtained by calibration at each light source. Here, the brightness value of a pure Lambertian surface can be described as:

$$A'_{max}((\vec{S} \cdot \vec{N}) + E_{lam}) \tag{11}$$

where $\vec{S}$ and $\vec{N}$ denote the light source direction Both the base value and the source brightness can be obtained by integrating appropriate equations. However, we will determine these parameters experimentally for the sake of accuracy.

These parameters are extracted by processing the 36 images of a pure Lambertian ball under 36 light sources independently. At each image, we sample, at 12°, a set of brightness values along the longitudinal great circle of the Lambertian sphere which passes through the light source direction. We can calculate $\vec{N} \cdot \vec{S}$ at each sampling point. Substituting these values and brightness values to Eq. 11, we can determine $A'_{max}$ and $E_{lam}$ by the least square fitting method.

When a surface normal makes an angle near $\pm 90°$ with respect to the light source direction, part of the extended light source is occluded by the surface itself. The brightness departs from the cosine curve. Therefore, only the brightness values given by the normal direction between $\pm 60°$ are used for this fitting.

The camera cannot see the entire area illuminated by an oblique direction of a source, due to occlusion by the Lambertian sphere. We can observe brightness only at the peripheral part of the cosine curve. In this case, the fitting method becomes unstable. Thus, we artificially generate a symmetric set of brightness with respect to the light source, and apply the least square fitting to the combined set of measured and the artificially generated brightness values.

## 3.4 Extraction Procedure

Image brightness at each pixel under the extended light source $i$ can be represented using the system parameters as:

$$I_i(\vec{N}, A', B') = A'(\vec{S}_i \cdot \vec{N} + E_{lamb}) + B'(L'(\vec{S}_i, \vec{N}) + E_{spec}) + E_{def} \qquad (12)$$

Here, the device characteristic parameters, $E_{lamb}, E_{spec}, E_{def}$, the light source direction $\vec{S}_i$, and the light source brightness for the pure Lambertian surface, $A'_{max}$ are given by the previous calibration procedure. The number of the light sources is 36. Namely, $i = 1, \ldots, 36$

We will recover $A', B', \vec{N}$ from step 1 through step 3 several times iteratively to obtain the accurate parameters. Before entering the main part of the iteration, we average the brightness values by using the following filter.

$$\begin{array}{ccc} 1 & 1 & 1 \\ 1 & 8 & 1 \\ 1 & 1 & 1 \end{array}$$

**Step 1: Cosine curve fitting** A measured brightness value, $I_i$ includes the three kinds of base values: Lambertian ($E_{lamb}$), specular ($E_{spec}$), and defocus ($E_{def}$). we subtract these base values from the brightness.

$$I'_i = I_i - E_{lamb}A' - E_{spec}B' - E_{def}.$$

In the initial iteration, $A'$ and $B'$ are unknown. Therefore, we set $A' = 0$ and $B' = 0$. After second iteration, we will substitute the values obtained at the previous iteration.

Then, the brightness is normalized by the the light source brightness for the pure Lambertian surface, $A'_{max,i}$, of source $i$ to compensate for the difference between the light sources.

Brightness values larger than a threshold (0.05) are considered as valid measurements and are used for fitting. This is because the actual photometric function of Lambertian surfaces does not follow a cosine curve in the peripheral area. If the number of valid measurements is larger than a threshold (currently, seven including the light sources on the specular triangle), the results of the fitting are regarded as valid and the surface orientation, $\vec{N}_{lamb}$, and the Lambertian strength, $A'$, are obtained. If not, the Lambertian component is considered not to exist.

**Step 2: Specular triangle determination** We subtract the base value and the Lambertian brightness values, extracted in the former step, from the measured brightness. We obtain the specular brightness as follows:

$$I''_i = I_i - A'\vec{S}_i \cdot \vec{N}_{lamb} - A'E_{lamb} - E_{def}.$$

Theoretically, three source directions, giving three largest specular brightness values, form the specular triangle. However, when the specular source direction of a surface patch agrees with the light source direction, the second and the third largest direction becomes unstable, and does not always belong to the same triangle.

In order to compensate this instability, we use the following procedure. We select the two largest brightness directions among the specular brightness, $(I''_i, i = 1, \ldots, 36)$. Usually, the two light sources of the largest values are adjacent with each other. In this case, the common edge of the sources belongs to two triangles. We will choose the one having the larger brightness at the third vertex, and form the specular triangle.

Sometimes, the two light sources giving maximum values are not adjacent with each other. In this case, we will pick the largest direction and search the next largest direction among the adjacent directions around it. We will form a common edge by the largest and the direction found in the previous search. Then, we will find the specular triangle among two triangles which shares the common edge.

**Step 3: Table lookup** The previous procedure gives the specular triangle, i.e. three specular brightness values, $I'_{i_1}, I'_{i_2}, I''_{i_3}$. In order to refer to the lookup table, we will normalize the specular brightness as

$$\begin{Bmatrix} I'''_{i_1} \\ I'''_{i_2} \\ I'''_{i_3} \end{Bmatrix} = \frac{k-1}{I''_{i_1} + I''_{i_2} + I''_{i_3}} \begin{Bmatrix} I''_{i_1} \\ I''_{i_2} \\ I''_{i_3} \end{Bmatrix}$$

where $k$ represents the total mesh number of an axis of the lookup table.

Using the normalized brightness, we can refer to the lookup table. In order to obtain accurate orientation, we will use the following interpolation method.

The first step generates 4 sets of indices around $I'''_{i_1}, I'''_{i_2}, I'''_{i_3}$:

$$(l, m, k-1-l-m),$$

$$(l+1, m, k-2-l-m),$$

$$(l, m+1, k-2-l-m),$$

$$(l+1, m+1, k-3-l-m)$$

where $l = [I'''_{i_1}]$, $m = [I'''_{i_2}]$ and $l_r = I'''_{i_1} - l$, $m_r = I'''_{i_2} - m$. See Figure 11.

The second step actually refers to the table using these indices. However, since some of the referred cells in the table may not contain orientation information, we will execute the following interpolation procedure.

- *Case 1:* When three or four cells, that are pointed to by the indices, contain orientations, interpolate between them by using the residue, $i_r$, $j_r$.
- *Case 2:* When one or two cells, pointed to by the indices, contain orientations, use those values without interpolation.
- *Case 3:* When none of the cells contains an orientation, send the failure signal.

Case 1 and 2 provide surface orientation, $N_{spec}$. By using this orientation, we calculate the specular source direction, $\vec{S}_n(\vec{N})$ of the orientation. Then, we find the nearest light source direction $\vec{S}_i$ from this direction, $\vec{S}_n(\vec{N})$. Substituting the source and specular direction in Eq. 10 gives the theoretical brightness. The specular albedo $B'$ is determined as the ratio of the measured specular and the theoretical brightness.

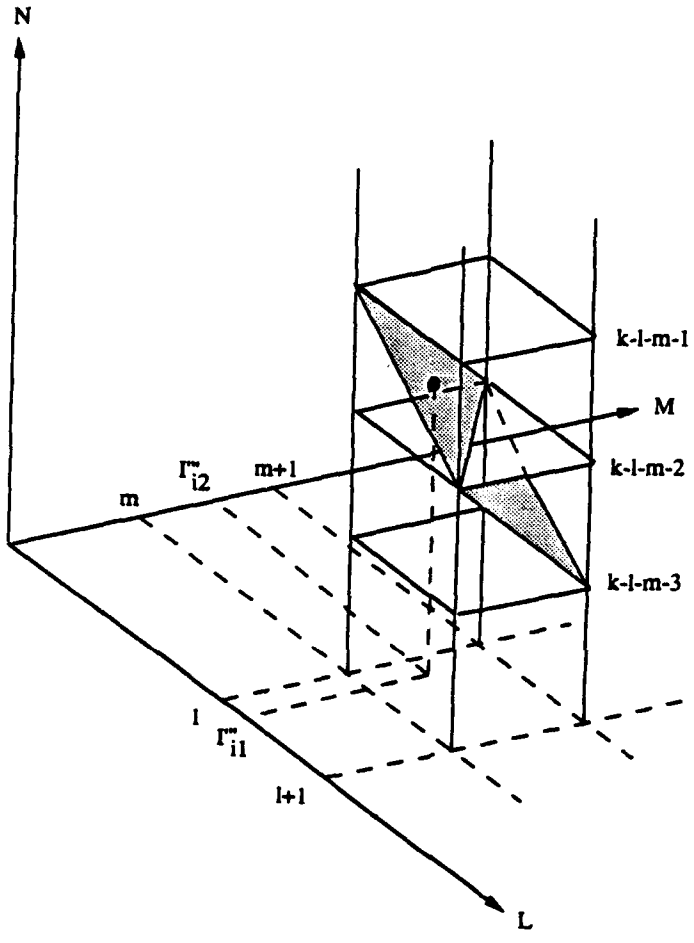


Figure 11: Interpolation method

# 4 Experimental Results

This section describes experiments conducted to evaluate the performance of the photosampling method. As explained previously, the method can extract shape and reflectance of Lambertian, specular, and hybrid surfaces. In order to evaluate the accuracy of the method, first, we measure three kinds of spherical surfaces, known shape and known reflectance: Lambertian, specular, and hybrid surfaces. Then, we applied the method to other interesting surfaces to demonstrate the feasibility of the method in practical applications as well as to investigate its limitations.

## 4.1 Specular spherical surface

Figure 12 shows a 0.5 inch diameter specular ball and its 36 images obtained using the photo-sampling device. By applying the extraction procedure to these images, we obtain the Lambertian strength as shown in Figure 13(a) and the specular strength as shown in Figure 13(b). The surface orientation distribution is obtained as shown in Figure 14(a), where a small needle depicts the orientation at that pixel. The detected error of the surface normals along the $X$ axis is shown in the Figure 14(c). We find that the errors are less than 1 degree in the central region of the ball.

Figure 14(b) shows the distribution of the errors in computed surface orientations. The figure indicates that the peripheral area has larger error than the central area. This tendency can be explained by the discrepancy of the actual brightness distribution of a light source from the theoretical one. Figure 15(a) and 15(b) shows the fitting results of the 25th light, which is located in the horizontal direction, and the 36th light, which has the maxmum angle with respect to the camera, as the examples of the fitting results at the peripheral area. The actual brightness distribution has larger discrepancy from the theoretical one in the longitudinal direction than the perpendicular direction as shown in the Figure 15.

The brightness in a pixel measured by a TV camera is the resu! of the integration of those over the corresponding area on the diffuser. On the other hand, the theoretical brightness is defined as multiplication of the pixel area with those at the center direction of the pixel. The variance in surface orientations within a pixel becomes larger in the circumference of the ball; thus the variance in brightness within a pixel increases in the circumference of the ball. A larger brightness variance causes more departure of the integrated brightness from those given by multiplication of the pixel area with those at the center of the pixel. This departure

causes a relatively larger error at the circumference. If the tables for specular surfaces are made directly from the brightness of the specular ball images, the accuracy will be improved.

We can also observe the systematic error distribution over the ball corresponding to the tessellations. The accuracy of an obtained surface orientation is related to the gradient of a brightness distribution function of an extended light source. A steeper portion of the function gives a more accurate orientation. The gradient of the source distribution function is not constant over a triangle. It becomes relatively flat around the peripheral area of a triangle. Consequently, errors increase in that region.

Therefore, it is desirable for the function to have a steep gradient at the peripheral area of a triangle. In order to achieve this condition, we should have a larger $\alpha$ than the width of a triangle. In other words, the distance between the light sources and the diffuser should be wider than those given by the design specification in Eq. 8.

## 4.2 Lambertian spherical surface

Figure 16 shows a 0.5 inch diameter matt-white painted Lambertian ball and its 36 images taken under our device. Figure 17(a) represents the Lambertian strength, and Figure 17(b) represents the specular strength. Figure 18(a) shows the orientation distribution depicted as a needle map.

Figure 18(b) shows the error distributions over the sphere. Figure 18(c) shows the error distributions along $x$ axis. The average error is 2% and the maxmum error is 3.5%. We can conclude that the Lambertian ball has larger errors in obtained orientations. This is because the cosine curve, the photometric function of a Lambertian surface, has more flat gradient than that for a pure specular surface.

In addition, the maxmum brightness of Lambertian surfaces is about only 20% of those of specular surfaces. Although we use extended light sources to detect both specular and Lambertian surfaces with the same order of brightness, to equate the maxmum brightness of Lambertian surface to those of specular surfaces requires that the termination angle be larger than 90°. Thus, we cannot realize such large termination angles[5].

[5]It is still reasonable to make Lambertian surfaces darker than specular surfaces because the Lambertian components are extracted from more data than specular components by using the least mean square fitting method which is stable with noise.

## 4.3 Hybrid spherical surface

Examples of the hybrid surfaces include smooth plastic and glossy painted surfaces. To examine the system performance on such hybrid surfaces, we use a glossy painted ball in this experiment. Figure 19 shows a 0.5 inch diameter glossy painted ball and its 36 images. Figure 20(a) and Figure 20(b) represent the Lambertian and specular strength, respectively. Figure 21(a) shows the needle map of the extracted surface normals. Figure 21(b) and Figure 21(c) depict error distributions in surface orientation of an entire sphere and along the x-axis, respectively.

## 4.4 Industrial object surface: Dip Switch

A dip switch, shown in Figure 22, is an example of the plastic object with a complicated shape. Figure 23(a) shows the Lambertian strength, Figure 23(b) shows the specular strength. As we expected, the system successfully obtained constant Lambertian strength distribution over the complicated shape. Although the switch has two different albedo areas, the distribution of the surface normals, depicted as the needle map in Figure 23(c), is seen not to be influenced by this albedo variation. However, concave and side areas are not detected correctly due to the occlusion. For example, the small circular concave on the switch is extracted with smaller albedo than actual, while the adjacent part to the switch is detected with inaccurate surface normal.

## 4.5 Solder Joint

Figure 24(a) shows a solder joint. Figure 24(b) shows the needle map of the surface normals.

## 4.6 Transparent surface

Transparent objects do not have a Lambertian component, but do have a specular component. As an example of a transparent surface, we have used the surface of a plastic lens as shown in Figure 25(a)

The plastic lens causes double reflections; a light ray hits the surface from the air to the plastic lens and a penetrated light ray hits the back surface from the plastic to the air. Figure 25(b) contains such double reflections.

In order to measure the only front reflection, we paint the lower surface with dull black spray. Figure 26 shows the result. Here, the length of each needle is multiplied by 5 times. The errors at the center is due to the hole of TV camera.

# 5 Conclusions

This paper describes a three-dimensional photometric sampling method to determine shape and reflectance of glossy surfaces by measuring image brightness under various light source directions and viewing from a single direction.

Extended light sources make it possible to ensure the detection of both Lambertian and specular reflections. We have distributed 36 light sources on the vertices of a one frequency icosahedron circumscribing a diffused sphere to generate evenly distributed extended light sources.

An extraction algorithm uses the set of image brightness values measured at each surface point in order to compute orientation as well as the strengths of the Lambertian and specular reflection components. In order to increase the accuracy in measured orientations and reflectance parameters, we have developed a calibration method to overcome the the difference between the theoretical and the actual distribution of extended source brightness.

The experimental results for Lambertian surfaces, specular surfaces, and hybrid surfaces show high accuracy in both orientations and reflectance parameters. We have demonstrated the ability of our system to detect surface orientations and reflectance parameter variations on a plastic and transparent surfaces, as well.

# Acknowledgements

Takeo Kanade provided many useful comments and encouragements. Mark DeLouis built the experimental apparatus. Fredric Solomon proofread drafts of this paper and provided many useful comments which have improved the readability of this paper. The authors also thank Yoshimasa Fujiwara for his valuable comments and Ye Mei for drawing several figures.

This research was conducted in the Task-oriented Vision Laboratory, Vision and Autonomous Center, the Robotics Institute, Carnegie Mellon University. Image Understanding Research in the TVL is supported in part by the Westinghouse Electric Corporation and in part by the Defense Advanced Research Project Agency, DOD, through ARPA order No. 4976, and monitored by the Air Force Avionics Laboratory under contract F33615-87-C-1499. Hideichi Sato was on leave of absence from Komatsu Ltd., Kanagawa, Japan.

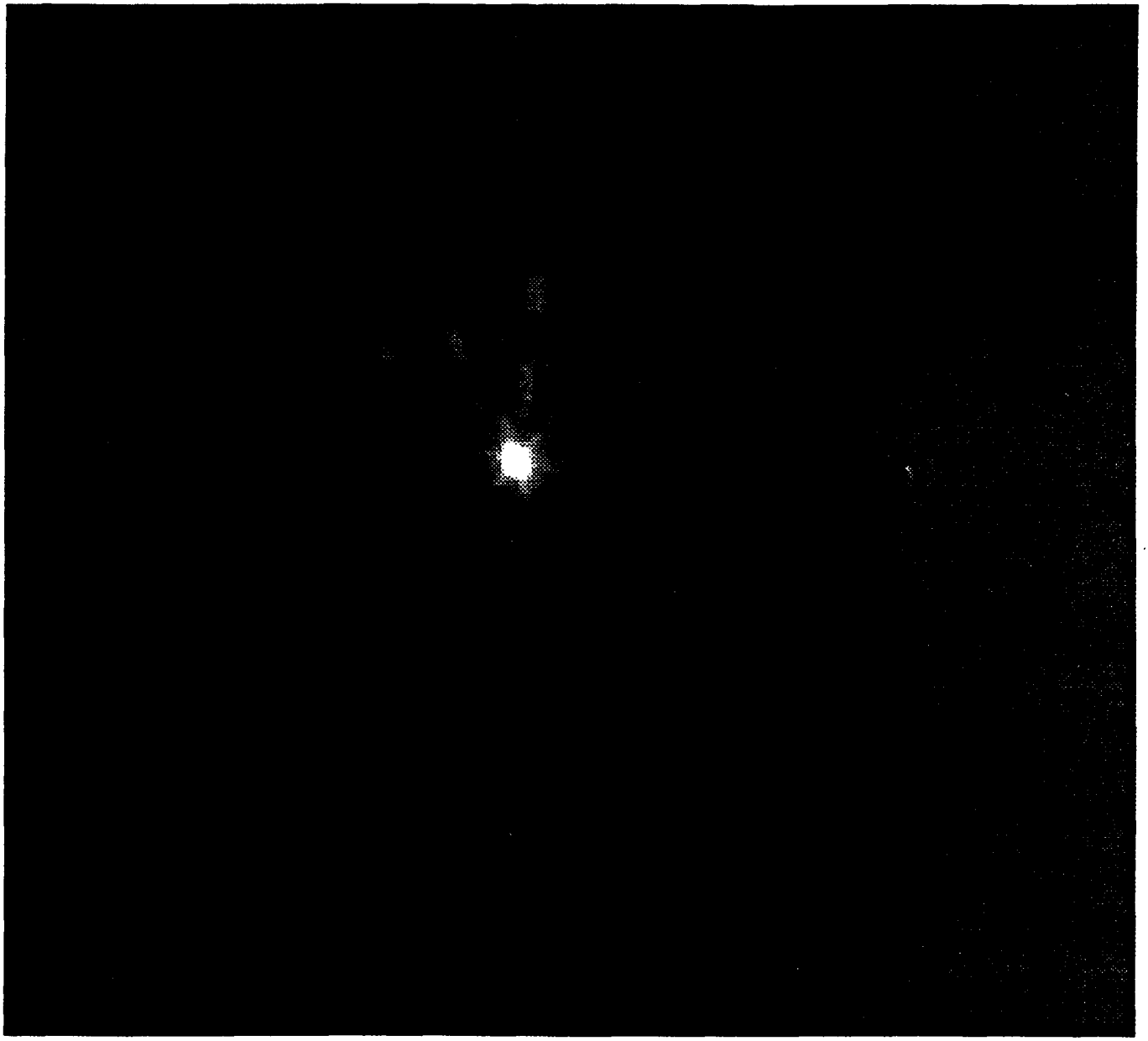

(a)

Figure 12: A specular ball; (a) Picture of a specular ball; (b) 36 images of the specular ball using the 3D photosampler.

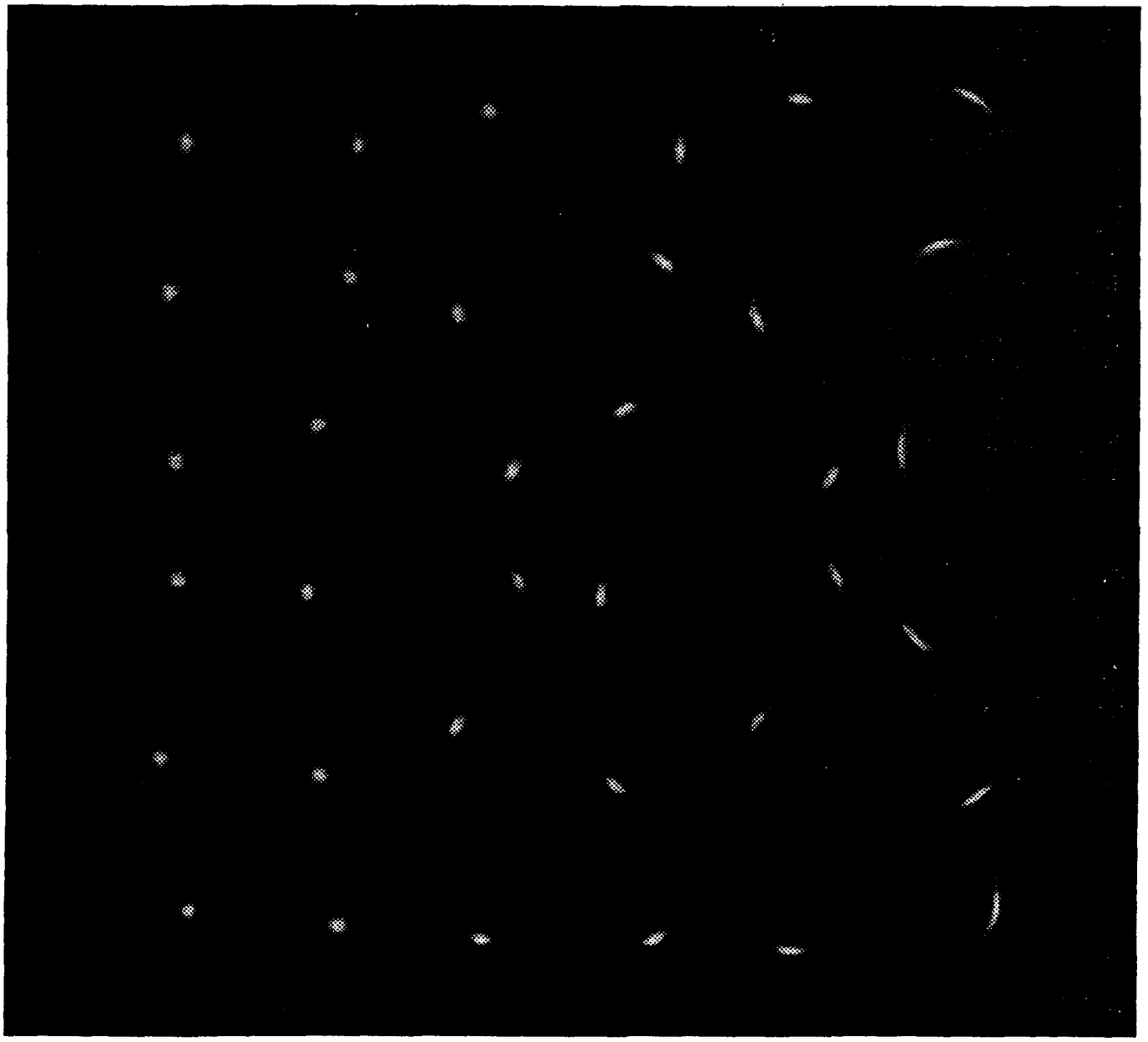

(b)

Figure 12 (cont)

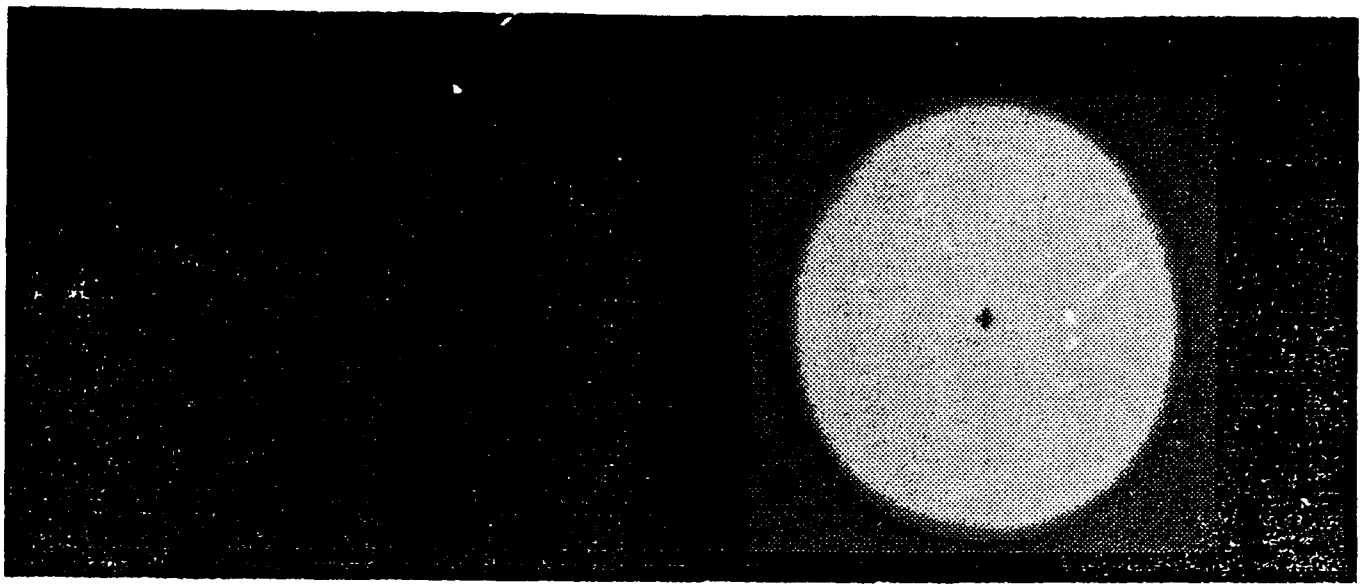

Figure 13: Strength images; (a) Lambertian strength image for the specular ball; (b) Specular strength image for the specular ball.

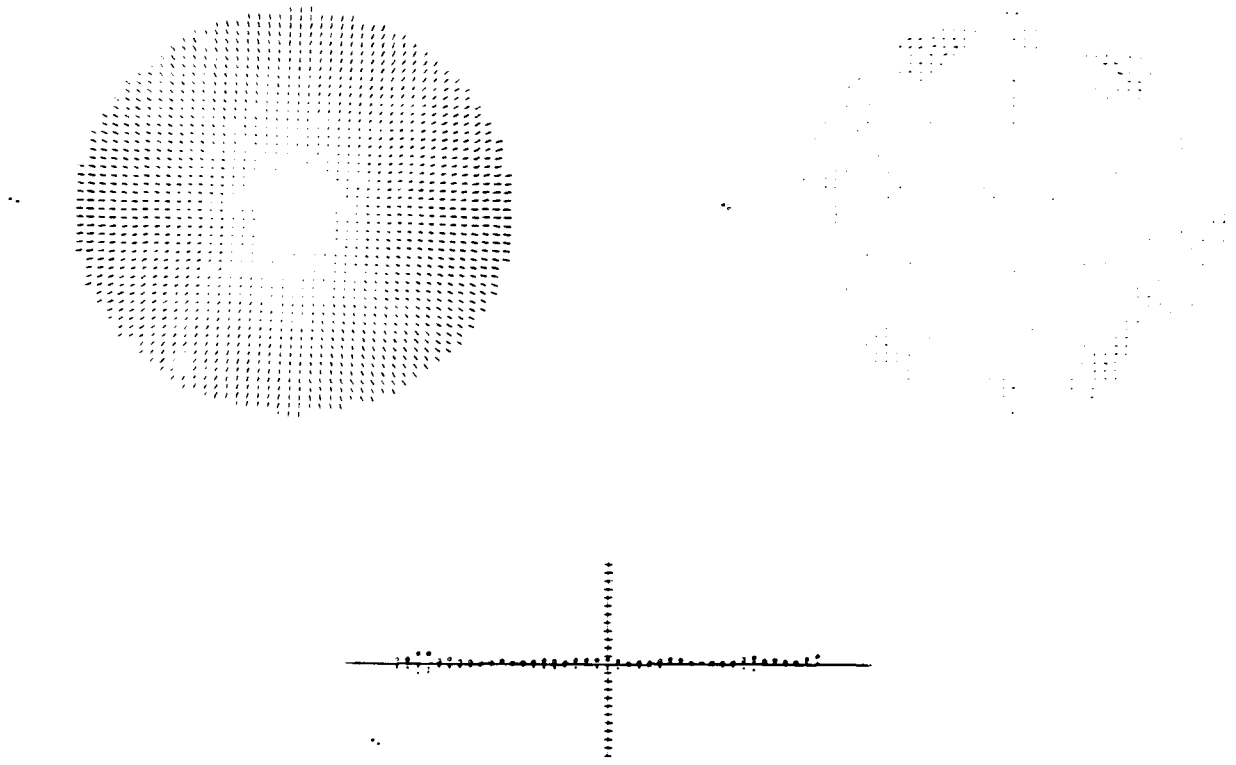

Figure 14: Needle map for the specular ball; (a) Needle map; (b) Needle map for the orientation error of the specular ball: the needle size is enhanced in 15 times; (c) The orientation error along the $x$ axis of the specular ball.

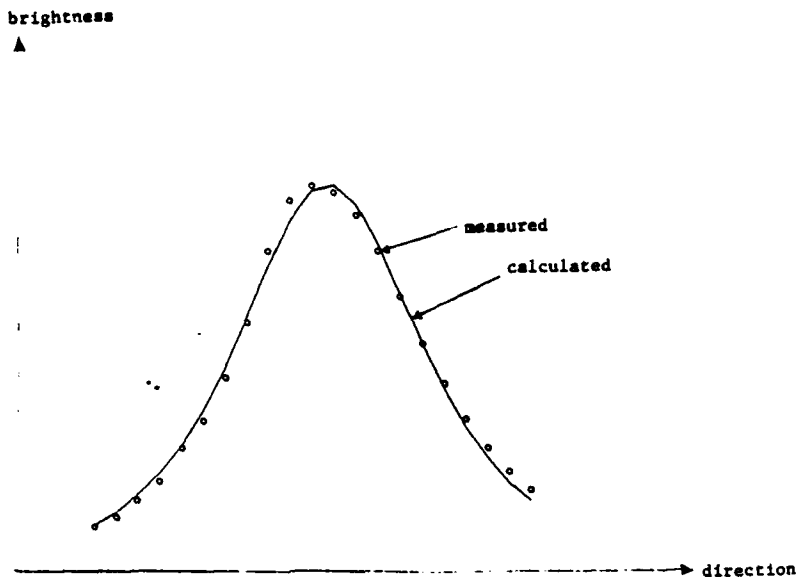


(a)

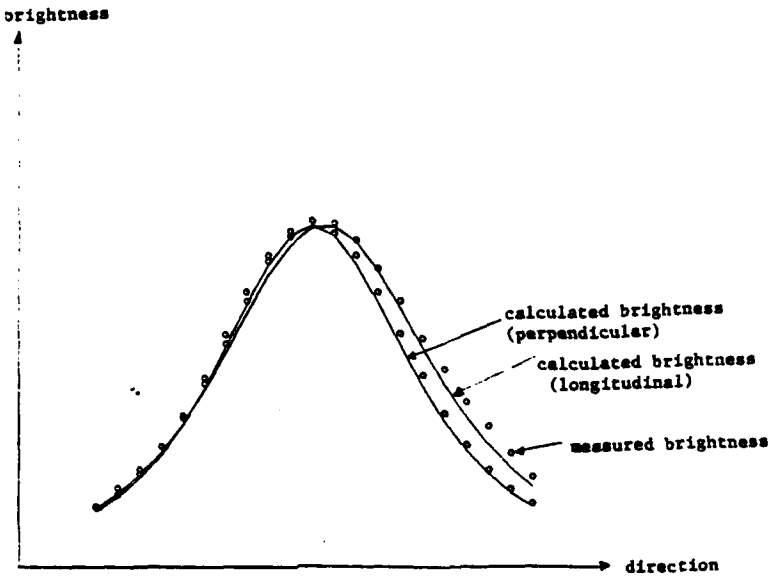


(b)

Figure 15: The fitting result; (a) The extended light source 25; (b) The extended light source 36.

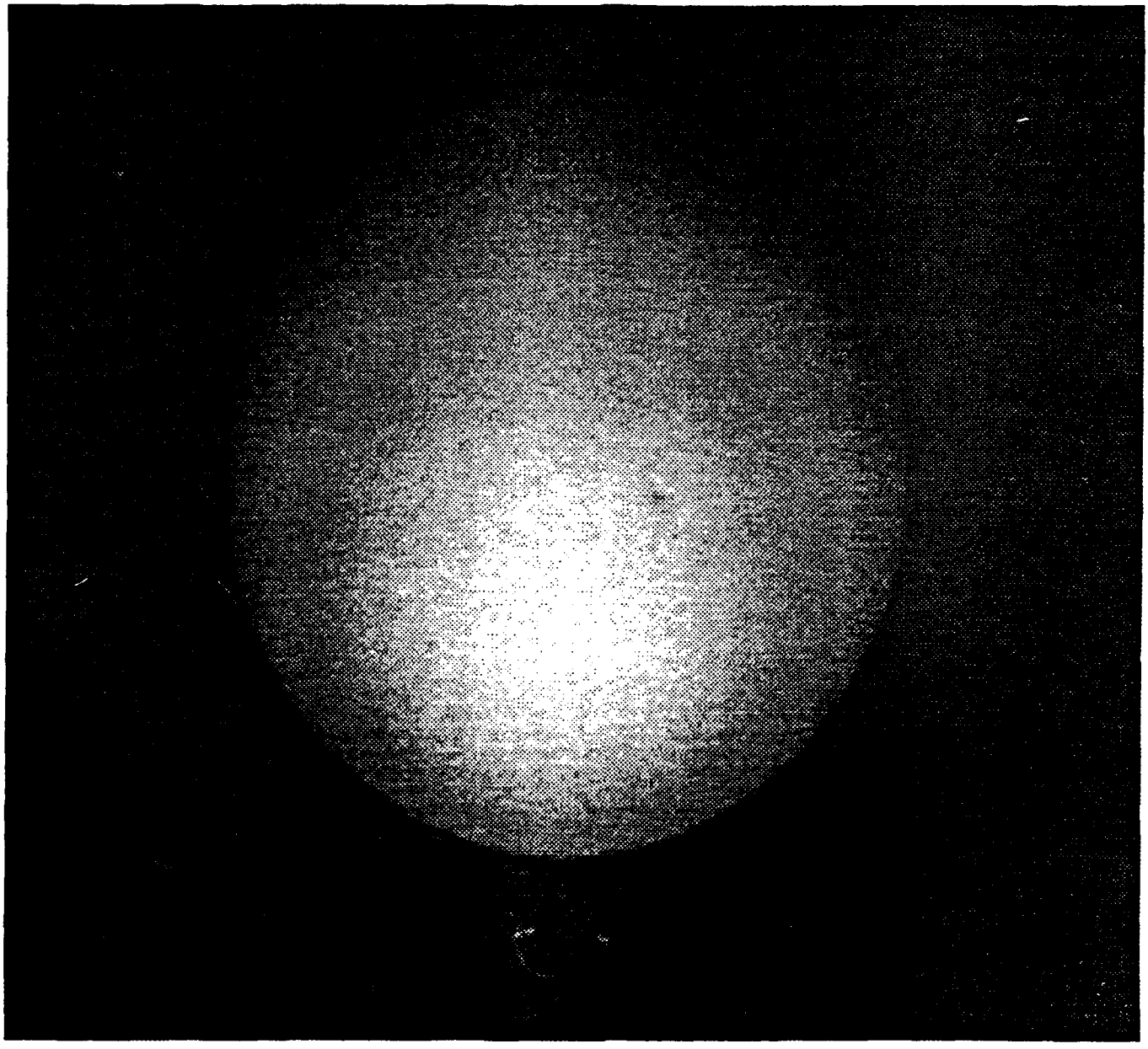

(a)

Figure 16: A Lambertian ball; (a) Picture of the Lambertian ball; (b) 36 images of a Lambertian ball under the photosampler.

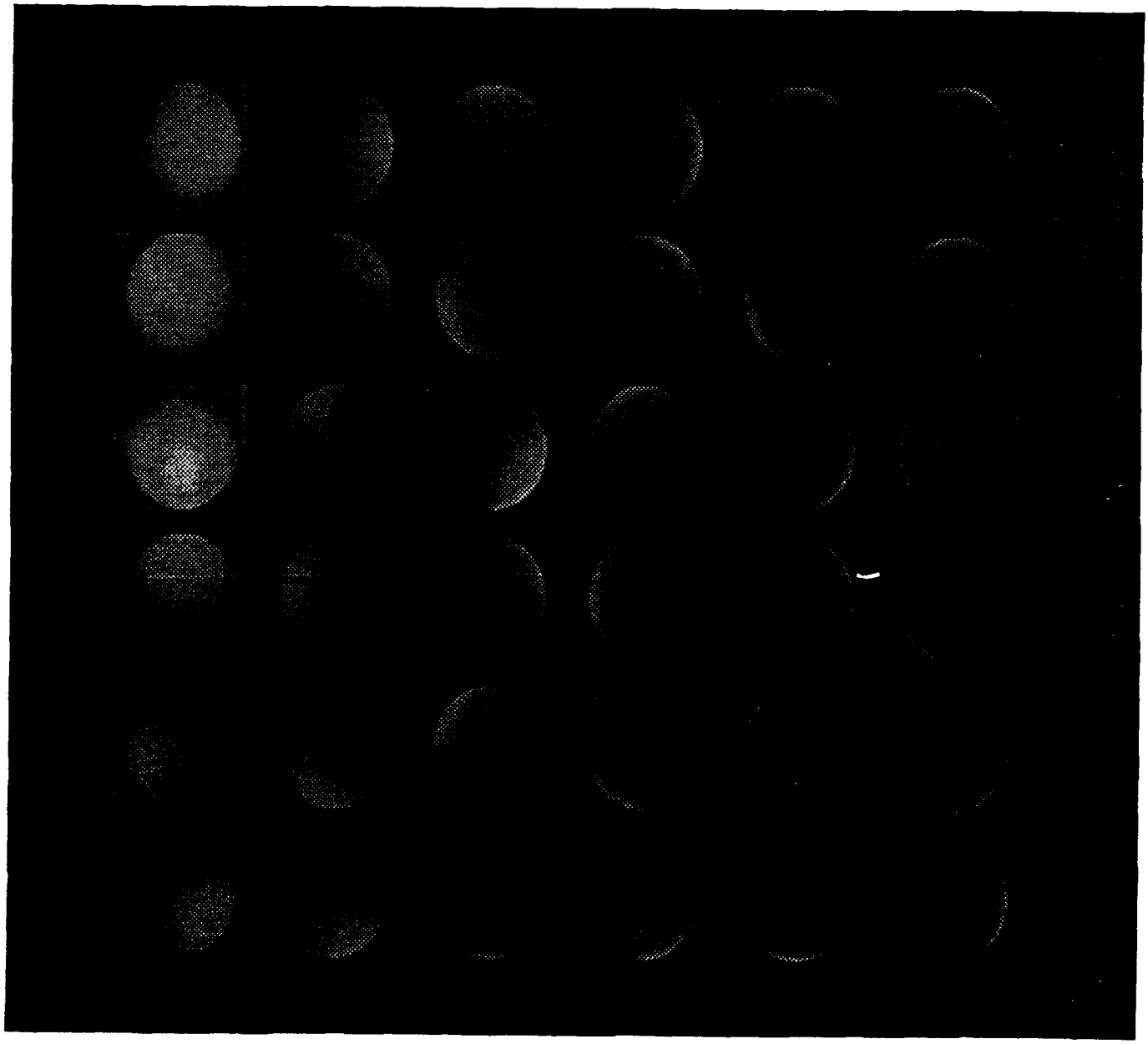

(b)

Figure 16 (cont)

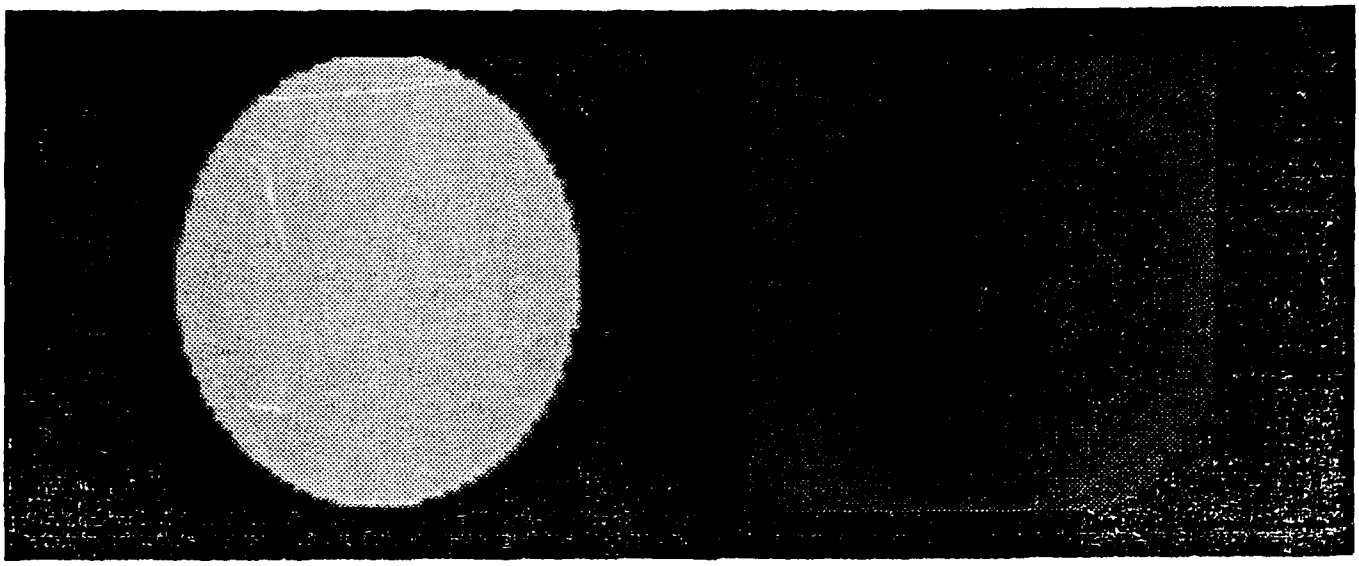

Figure 17: Strength images; (a) Lambertian strength image for the Lambertian ball; (b) Specular strength image for the Lambertian ball.

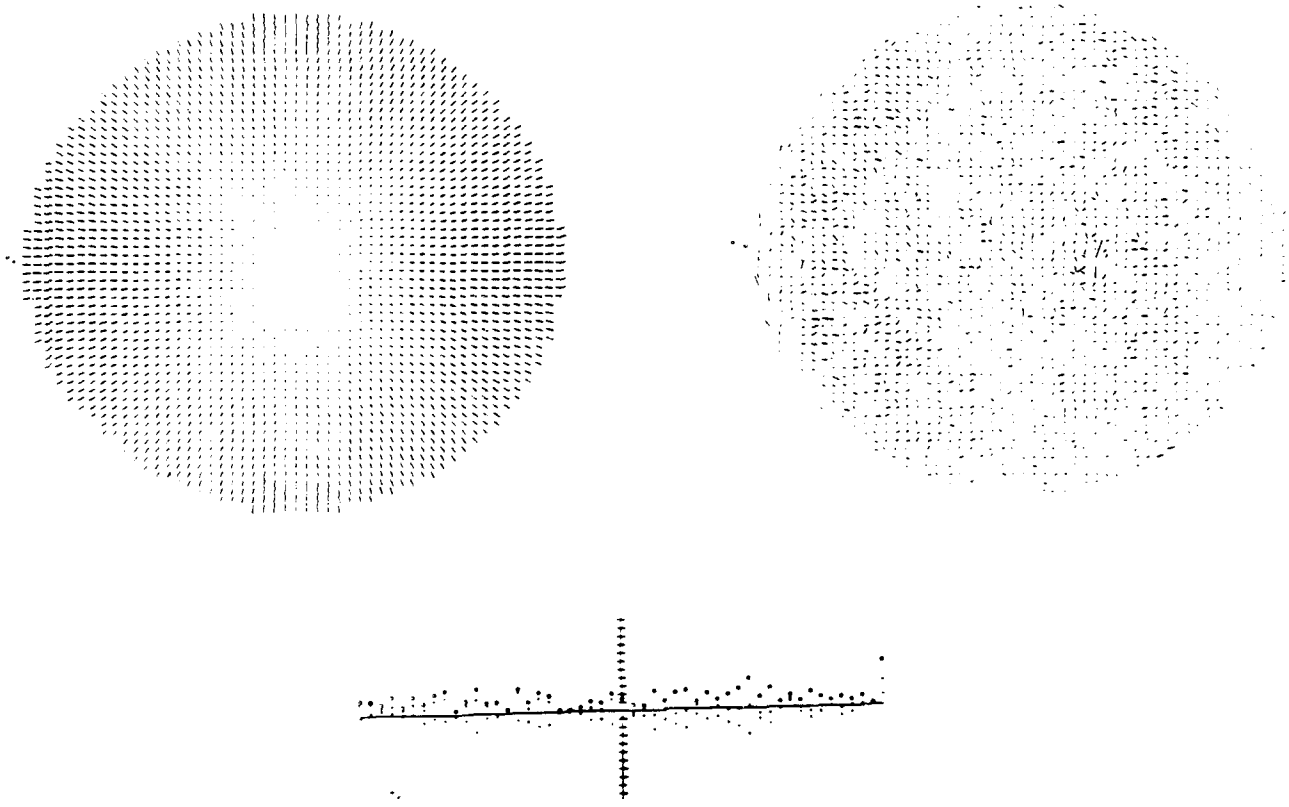

Figure 18: Needle map; (a) Needle map of the Lambertian ball; (b) Orientation errors of the Lambertian ball. Each length is multiplied by 15; (c) The orientation error along the $x$ axis of the Lambertian ball.

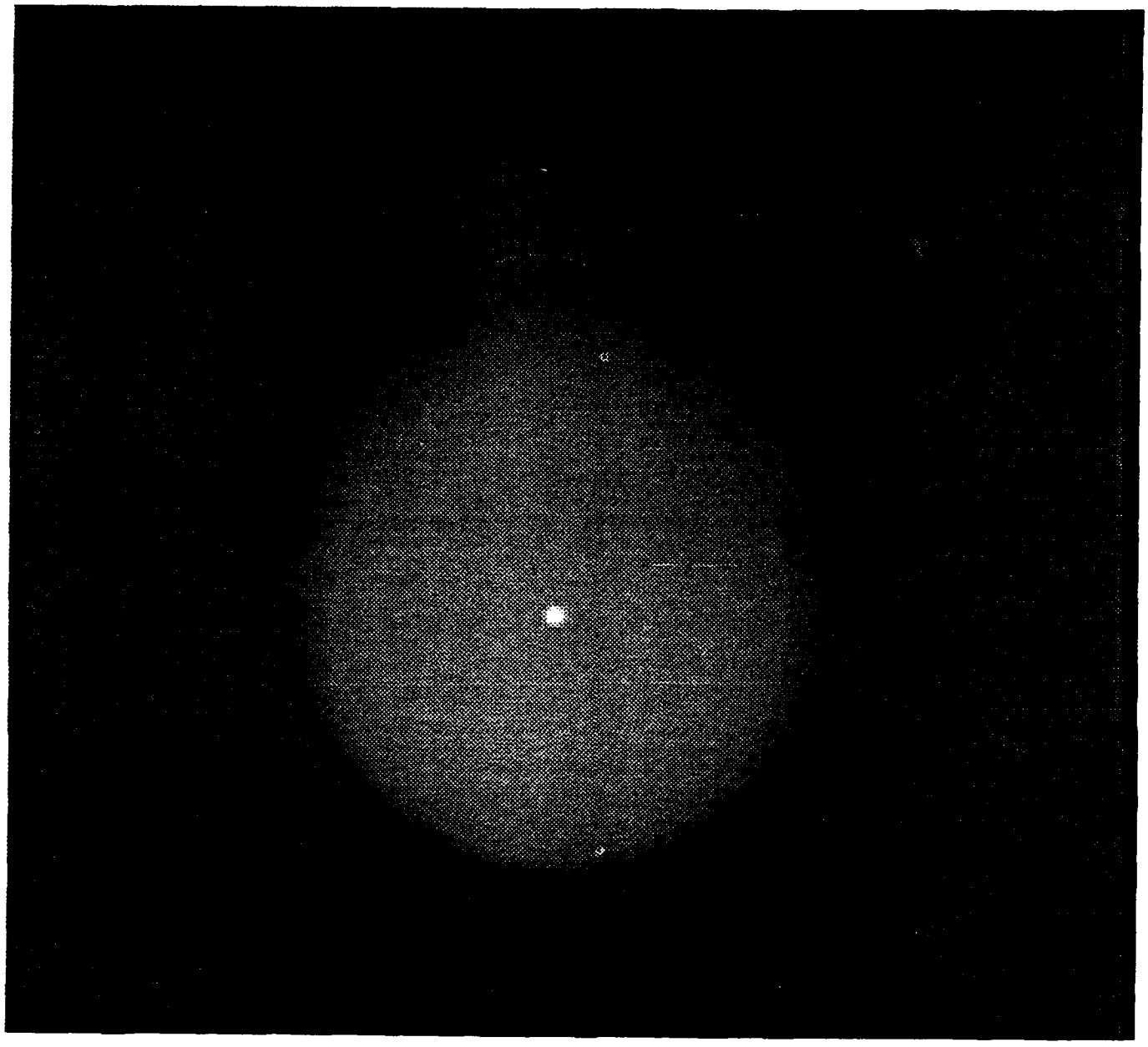

(a)

Figure 19: A painted ball (hybrid surface); (a) Picture of the ball; (b) 36 images of the ball.

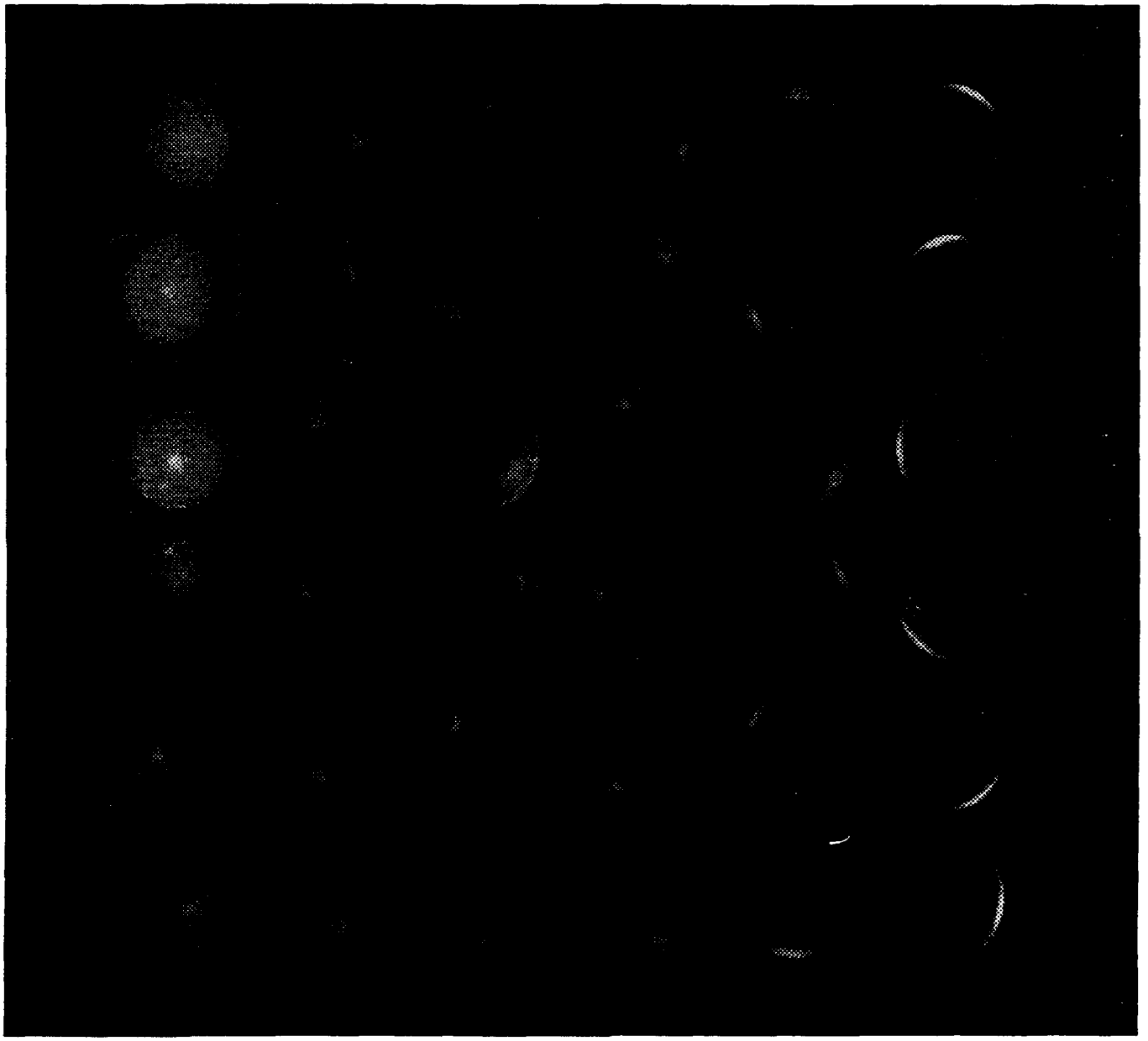

(b)

Figure 19 (cont)

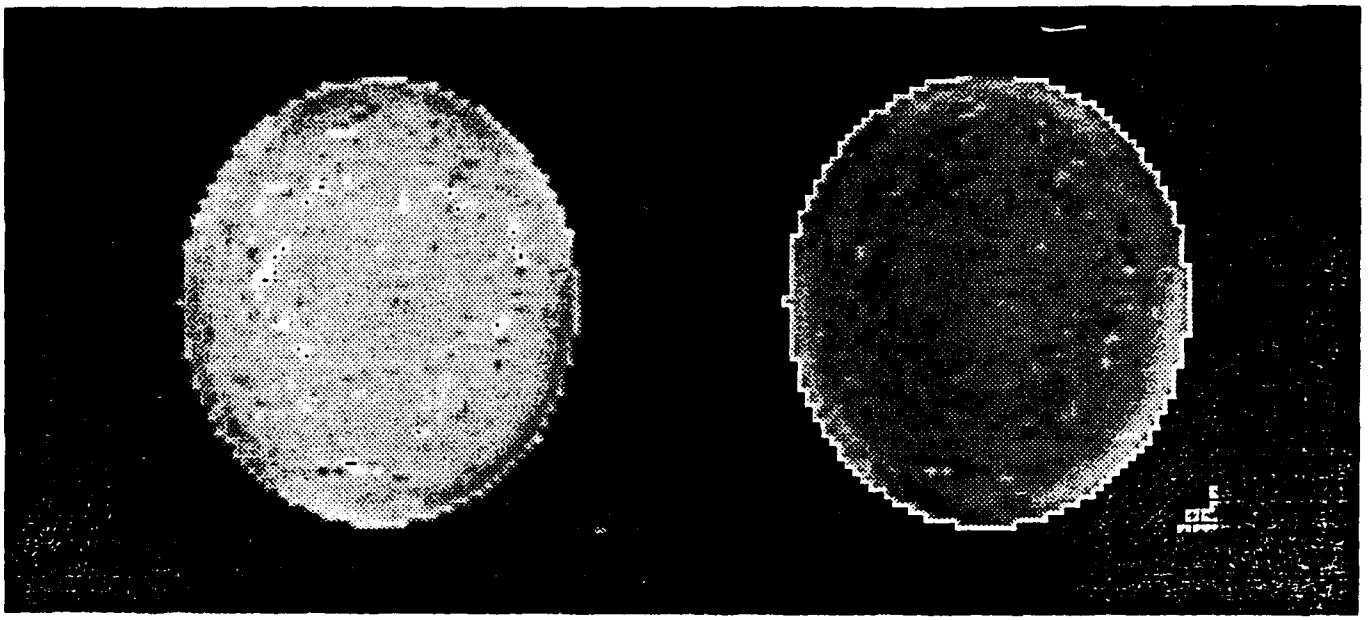

Figure 20: Strength images; (a) Lambertian strength image of the painted ball; (b) Specular strength image of the painted ball.

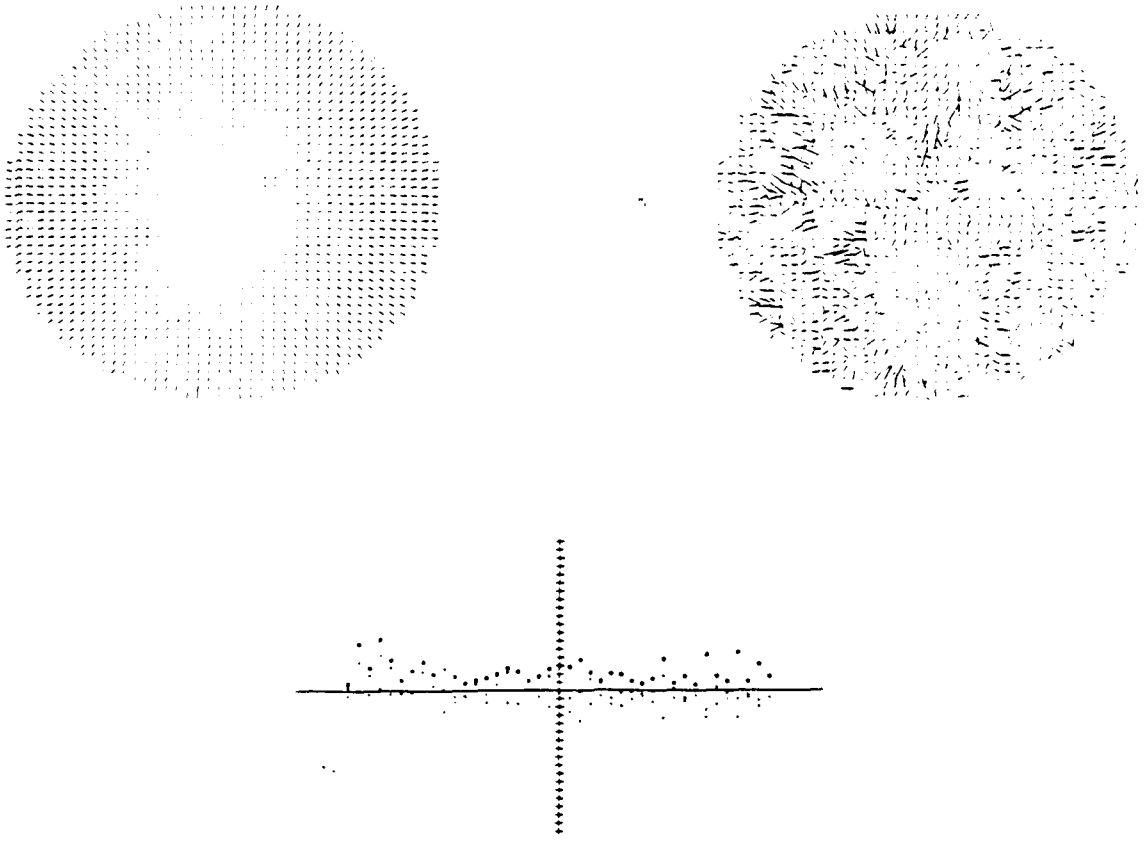

Figure 21: Needle map of the painted ball; (a) Needle map; (b) Error distribution; (c) The orientation error along the $x$ axis of the painted ball.

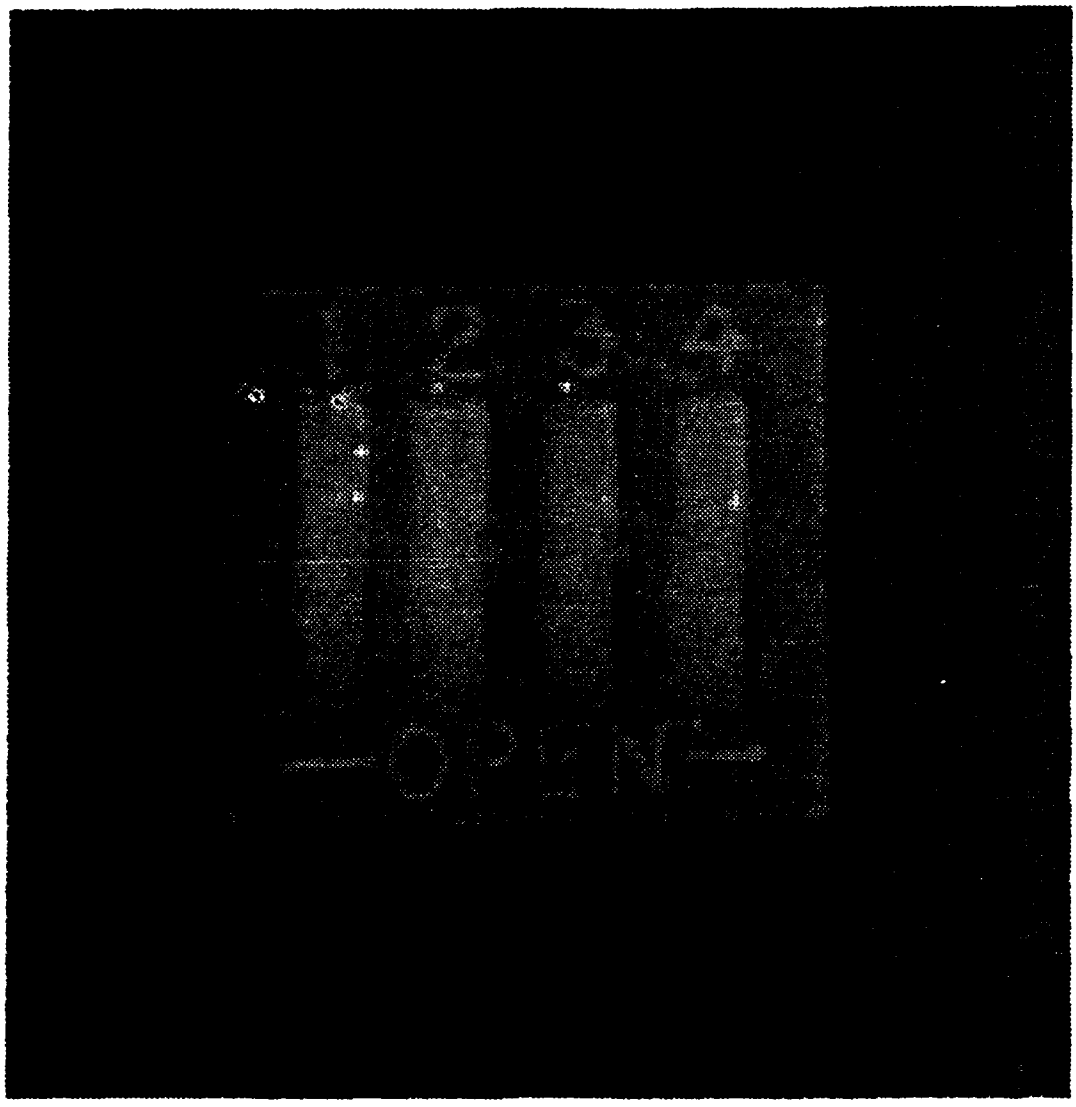

Figure 22: Picture of a dip switch.

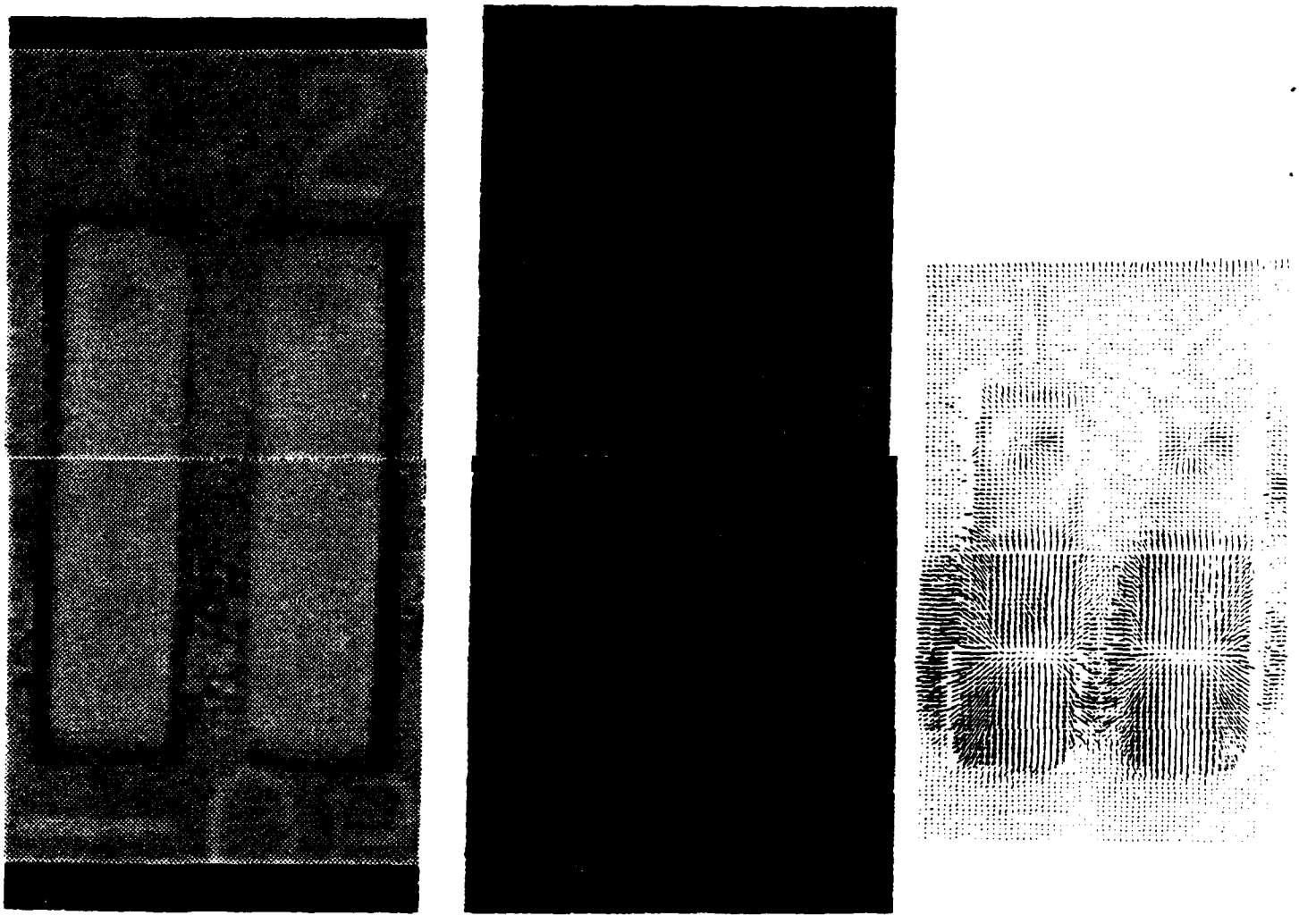


Figure 23: Result images: (a) Lambertian strength image for the dip switch; (b) Specular strength image for the dip switch; (c) Needle map of the dip switch.

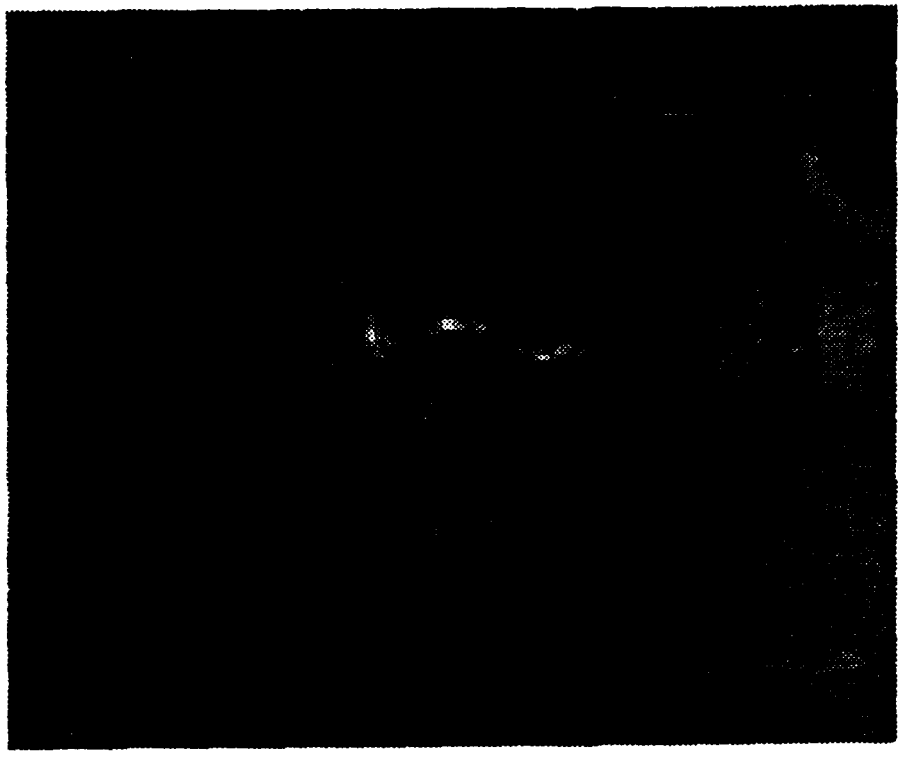

(a)

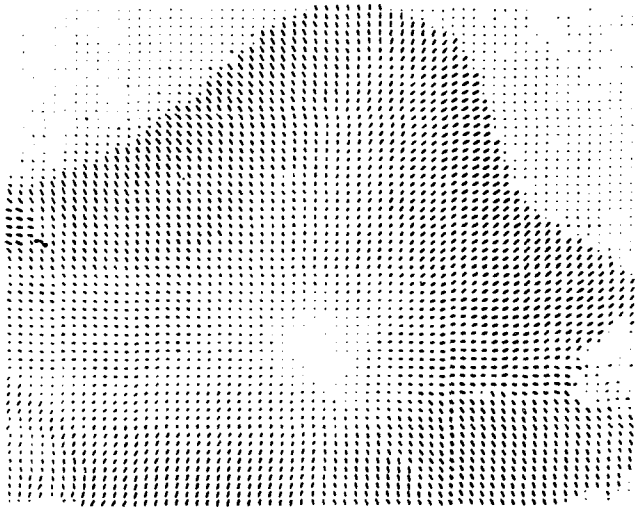

(b)

Figure 24: A solder joint; (a) Picture of a solder joint; (b) Needle map for the solder joint.

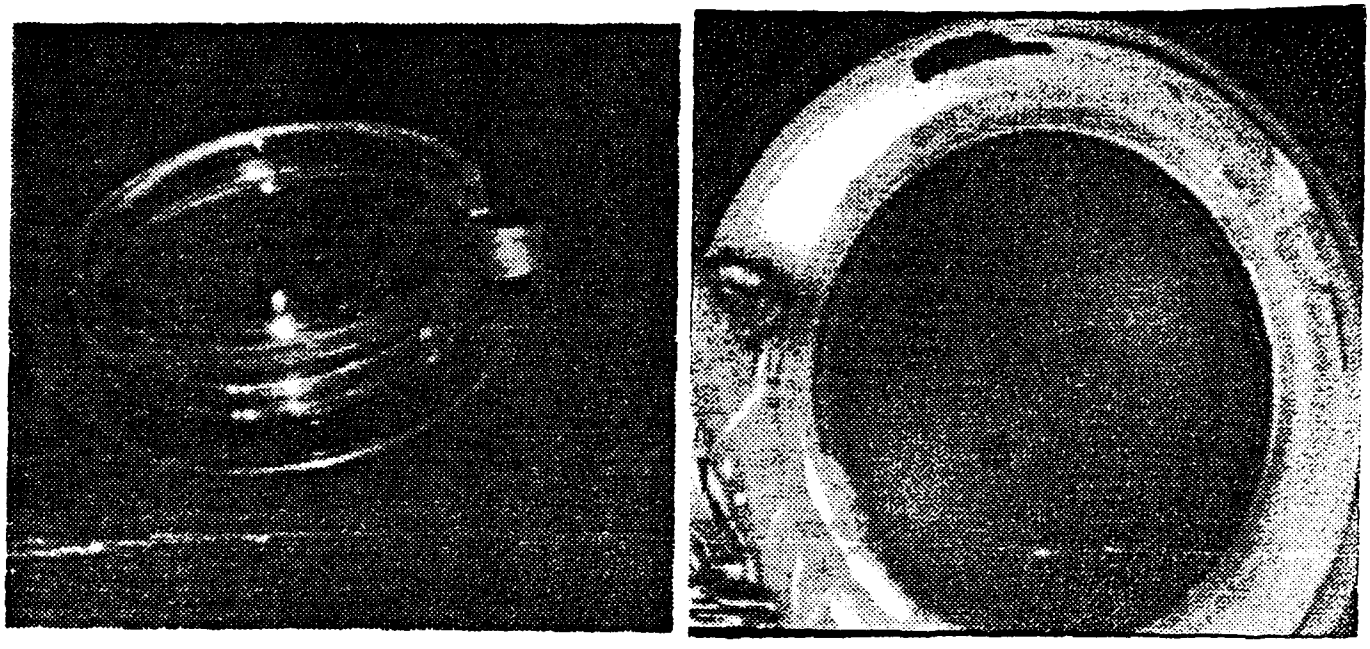

(a) (b)

Figure 25: Plastic lens: (a) Picture of a plastic lens; (b) two reflections are observed on the plastic lens.

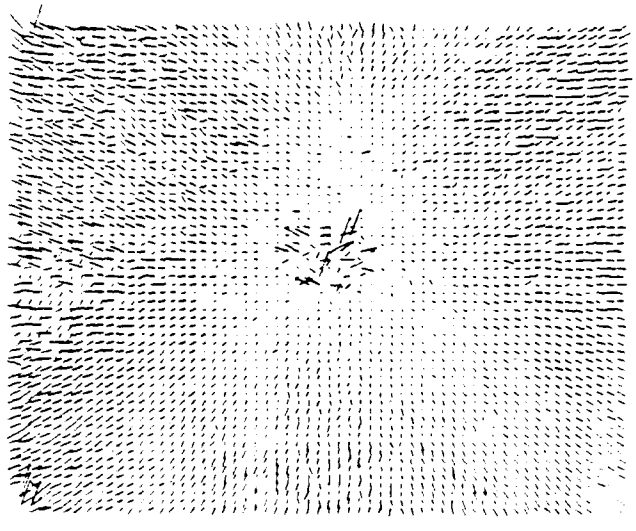

Figure 26: Needle map of the plastic lens.

# References


[1] C. Brown. Fast display of well-tessellated surfaces. *Computer and Graphics*, 4(4):77–85, April 1979.

[2] E.N. Coleman and Jain. R. Obtaining 3-dimensional shape of textured and specular surface using four-source photometry. *Computer Graphics and Image Processing*, 18(4):309–328, 1982.

[3] G. Healey and T.O. Binford. Local shape from specularity. *Computer Vision, Graphics, and Image Processing*, 42:62–86, 1988.

[4] B.K.P. Horn. Obaining shape from shading. In P.H. Winston, editor, *The Psychology of Computer Vision*, pages 115–155. McGraw-Hill, New York, 1975.

[5] K. Ikeuchi. Determining surface orientation of specular surfaces by using the photometric stereo method. *IEEE Trans. Pattern Analysis and Machine Intelligence*, PAMI-3(6):661–669, November 1981.

[6] K. Ikeuchi. Recognition of 3-d objects using the extended gaussian image. In *International Joint Conf. on Artificial Intelligence*, pages 595–600, 1981.

[7] K. Ikeuchi and K. Sato. Determining reflectance parameters using range and brightness images. In *Proc. of Intern. Conf. on Computer Vision*, Osaka, JAPAN, December 1990. a longer version is avaiable as CMU-CS-90-106.

[8] G.J. Klinker, S.A. Shafer, and T. Kanade. The measurement of highlights in color image. *Intern. Journal of Computer Vision*, 2(1), 1988.

[9] S.K. Nayar, K. Ikeuchi, and T. Kanade. Extracting shape and reflectance of lambertian, specular, and hybrid surfaces. Technical Report CMU-RI-TR-88-14, Carnegie Mellon University, Robotics Institute, August 1988.

[10] S.K. Nayar, K. Ikeuchi, and T. Kanade. Surface reflection: physical and geometrical perspectives. Technical Report CMU-RI-TR-89-7, Carnegie Mellon University, Robotics Institute, March 1989.

[11] A.P. Pentland. Local shading analysis. *IEEE Trans Pattern Analysis and Machine Intelligence*, PAMI-6(2):170–187, March 1984.

[12] A.C. Sanderson, L.E. Weiss, and S.K. Nayar. Structured highlight inspection of specular surfaces. *IEEE Trans. on Pattern Analysis and Machine Intelligence*, 10(1):44–55, January 1988.

[13] M.J. Wenninger. *Spherical Models*. Cambridge Univ. Press, Cambridge, UK, 1979.

[14] L.B. Wolff. Spectral and polarization stereo methods using a single light source. In *Proc. of DARPA Image Understanding Workshop*, pages 810–820. Science Application Inc., February 1987.

[15] L.B. Wolff. Using polarization to separate reflection components. In *Proc. of IEEE Conf. on Computer Vision and Pattern Recognition*, pages 363–369, 1989.

[16] R.J. Woodham. Reflectance map techniques for analyzing surface defects in metal castings. Technical Report AI-TR-457, Massachusetts Institute of Technology, Artificial Intelligence Laboratory, Cambridge, MA, 1978.